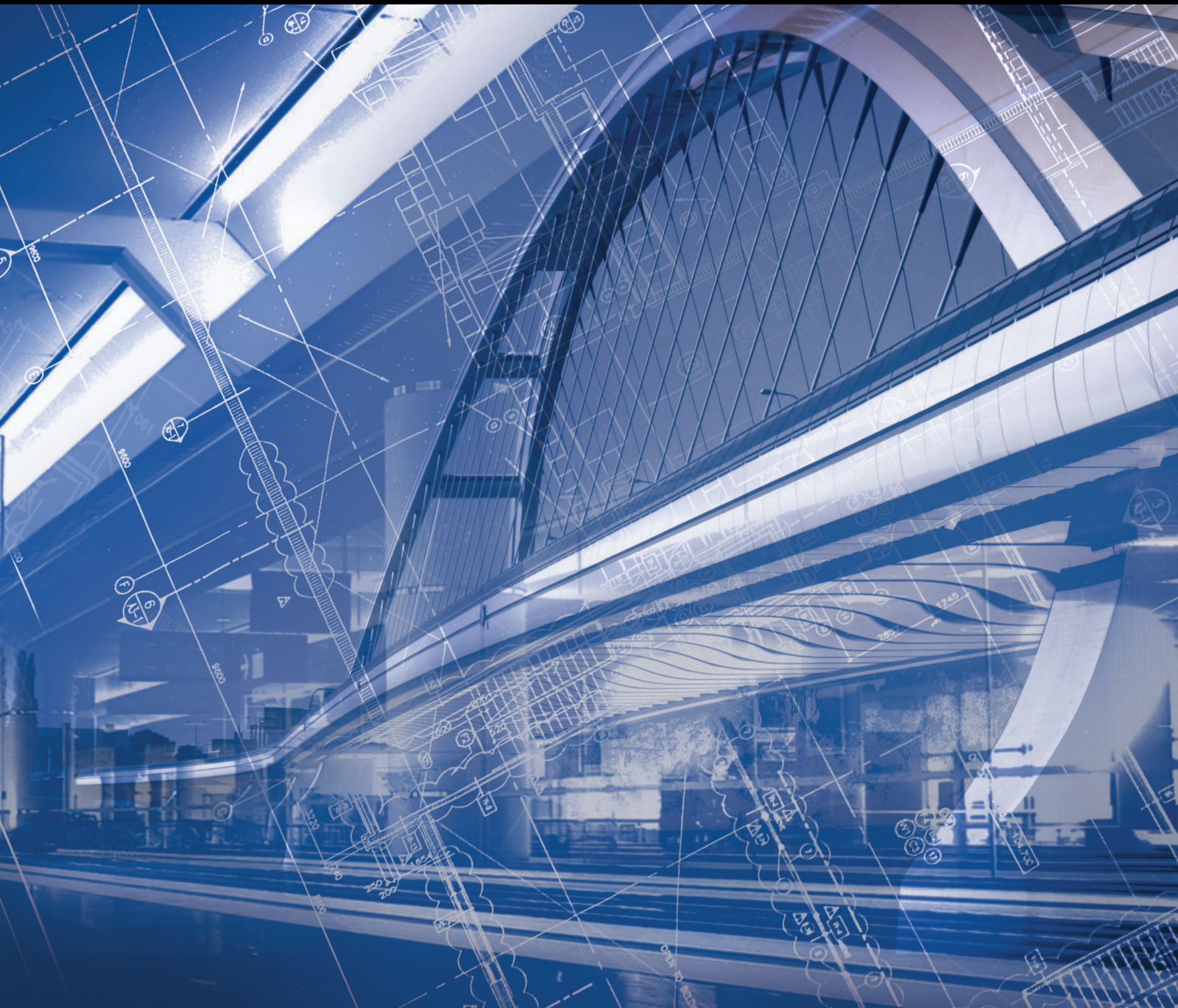


Advances in Civil Engineering

# Advances in the Research of Plates and Shells

Lead Guest Editor: Domagoj Matesan

Guest Editors: Giovanni Garcea and Roberto Nascimbene



---



# **Advances in the Research of Plates and Shells**



Advances in Civil Engineering

---

## **Advances in the Research of Plates and Shells**

Lead Guest Editor: Domagoj Matesan

Guest Editors: Giovanni Garcea and Roberto Nascimbene



Copyright © 2022 Hindawi Limited. All rights reserved.

This is a special issue published in "Advances in Civil Engineering." All articles are open access articles distributed under the Creative Commons Attribution License, which permits unrestricted use, distribution, and reproduction in any medium, provided the original work is properly cited.








# Chief Editor

Cumaraswamy Vipulanandan, USA













## Associate Editors

Chiara Bedon , Italy  
Constantin Chalioris , Greece  
Ghassan Chehab , Lebanon  
Ottavia Corbi, Italy  
Mohamed ElGawady , USA  
Husnain Haider , Saudi Arabia  
Jian Ji , China  
Jiang Jin , China  
Shazim A. Memon , Kazakhstan  
Hossein Moayedi , Vietnam  
Sanjay Nimbalkar, Australia  
Giuseppe Oliveto , Italy  
Alessandro Palmeri , United Kingdom  
Arnaud Perrot , France  
Hugo Rodrigues , Portugal  
Victor Yepes , Spain  
Xianbo Zhao , Australia

## Academic Editors

José A.F.O. Correia, Portugal  
Glenda Abate, Italy  
Khalid Abdel-Rahman , Germany  
Ali Mardani Aghabaglou, Turkey  
José Aguiar , Portugal  
Afaq Ahmad , Pakistan  
Muhammad Riaz Ahmad , Hong Kong  
Hashim M.N. Al-Madani , Bahrain  
Luigi Aldieri , Italy  
Angelo Aloisio , Italy  
Maria Cruz Alonso, Spain  
Filipe Amarante dos Santos , Portugal  
Serji N. Amirkhania, USA  
Eleftherios K. Anastasiou , Greece  
Panagiotis Ch. Anastasopoulos , USA  
Mohamed Moafak Arbili , Iraq  
Farhad Aslani , Australia  
Siva Avudaiappan , Chile  
Ozgur BASKAN , Turkey  
Adewumi Babafemi, Nigeria  
Morteza Bagherpour, Turkey  
Qingsheng Bai , Germany  
Nicola Baldo , Italy  
Daniele Baraldi , Italy

Eva Barreira , Portugal  
Emilio Bastidas-Arteaga , France  
Rita Bento, Portugal  
Rafael Bergillos , Spain  
Han-bing Bian , China  
Xia Bian , China  
Huseyin Bilgin , Albania  
Giovanni Biondi , Italy  
Hugo C. Biscaia , Portugal  
Rahul Biswas , India  
Edén Bojórquez , Mexico  
Giosuè Boscato , Italy  
Melina Bosco , Italy  
Jorge Branco , Portugal  
Bruno Briseghella , China  
Brian M. Broderick, Ireland  
Emanuele Brunesi , Italy  
Quoc-Bao Bui , Vietnam  
Tan-Trung Bui , France  
Nicola Buratti, Italy  
Gaochuang Cai, France  
Gladis Camarini , Brazil  
Alberto Campisano , Italy  
Qi Cao, China  
Qixin Cao, China  
Iacopo Carnacina , Italy  
Alessio Cascardi, Italy  
Paolo Castaldo , Italy  
Nicola Cavalagli , Italy  
Liborio Cavaleri , Italy  
Anush Chandrappa , United Kingdom  
Wen-Shao Chang , United Kingdom  
Muhammad Tariq Amin Chaudhary, Kuwait  
Po-Han Chen , Taiwan  
Qian Chen , China  
Wei Tong Chen , Taiwan  
Qixiu Cheng, Hong Kong  
Zhanbo Cheng, United Kingdom  
Nicholas Chileshe, Australia  
Prinya Chindaprasirt , Thailand  
Corrado Chisari , United Kingdom  
Se Jin Choi , Republic of Korea  
Heap-Yih Chong , Australia  
S.H. Chu , USA  
Ting-Xiang Chu , China

Zhaofei Chu , China  
Wonseok Chung , Republic of Korea  
Donato Ciampa , Italy  
Gian Paolo Cimellaro, Italy  
Francesco Colangelo, Italy  
Romulus Costache , Romania  
Liviu-Adrian Cotfas , Romania  
Antonio Maria D'Altri, Italy  
Bruno Dal Lago , Italy  
Amos Darko , Hong Kong  
Arka Jyoti Das , India  
Dario De Domenico , Italy  
Gianmarco De Felice , Italy  
Stefano De Miranda , Italy  
Maria T. De Risi , Italy  
Tayfun Dede, Turkey  
Sadik O. Degertekin , Turkey  
Camelia Delcea , Romania  
Cristoforo Demartino, China  
Giuseppe Di Filippo , Italy  
Luigi Di Sarno, Italy  
Fabio Di Trapani , Italy  
Aboelkasim Diab , Egypt  
Thi My Dung Do, Vietnam  
Giulio Dondi , Italy  
Jiangfeng Dong , China  
Chao Dou , China  
Mario D'Aniello , Italy  
Jingtao Du , China  
Ahmed Elghazouli, United Kingdom  
Francesco Fabbrocino , Italy  
Flora Faleschini , Italy  
Dingqiang Fan, Hong Kong  
Xueping Fan, China  
Qian Fang , China  
Salar Farahmand-Tabar , Iran  
Ilenia Farina, Italy  
Roberto Fedele, Italy  
Guang-Liang Feng , China  
Luigi Fenu , Italy  
Tiago Ferreira , Portugal  
Marco Filippo Ferrotto, Italy  
Antonio Formisano , Italy  
Guoyang Fu, Australia  
Stefano Galassi , Italy


Junfeng Gao , China  
Meng Gao , China  
Giovanni Garcea , Italy  
Enrique García-Macías, Spain  
Emilio García-Taengua , United Kingdom  
DongDong Ge , USA  
Khaled Ghaedi, Malaysia  
Khaled Ghaedi , Malaysia  
Gian Felice Giaccu, Italy  
Agathoklis Giaralis , United Kingdom  
Ravindran Gobinath, India  
Rodrigo Gonçalves, Portugal  
Peilin Gong , China  
Belén González-Fonteboa , Spain  
Salvatore Grasso , Italy  
Fan Gu, USA  
Erhan Güneyisi , Turkey  
Esra Mete Güneyisi, Turkey  
Pingye Guo , China  
Ankit Gupta , India  
Federico Gusella , Italy  
Kemal Hacıfendioglu, Turkey  
Jianyong Han , China  
Song Han , China  
Asad Hanif , Macau  
Hadi Hasanzadehshooiili , Canada  
Mostafa Fahmi Hassanein, Egypt  
Amir Ahmad Hedayat , Iran  
Khandaker Hossain , Canada  
Zahid Hossain , USA  
Chao Hou, China  
Biao Hu, China  
Jiang Hu , China  
Xiaodong Hu, China  
Lei Huang , China  
Cun Hui , China  
Bon-Gang Hwang, Singapore  
Jijo James , India  
Abbas Fadhil Jasim , Iraq  
Ahad Javanmardi , China  
Krishnan Prabhakan Jaya, India  
Dong-Sheng Jeng , Australia  
Han-Yong Jeon, Republic of Korea  
Pengjiao Jia, China  
Shaohua Jiang , China



MOUSTAFA KASSEM , Malaysia  
Mosbeh Kaloop , Egypt  
Shankar Karuppanan , Ethiopia  
John Kechagias , Greece  
Mohammad Khajehzadeh , Iran  
Afzal Husain Khan , Saudi Arabia  
Mehran Khan , Hong Kong  
Manoj Khandelwal, Australia  
Jin Kook Kim , Republic of Korea  
Woosuk Kim , Republic of Korea  
Vaclav Koci , Czech Republic  
Loke Kok Foong, Vietnam  
Hailing Kong , China  
Leonidas Alexandros Kouris , Greece  
Kyriakos Kourousis , Ireland  
Moacir Kripka , Brazil  
Anupam Kumar, The Netherlands  
Emma La Malfa Ribolla, Czech Republic  
Ali Lakirouhani , Iran  
Angus C. C. Lam, China  
Thanh Quang Khai Lam , Vietnam  
Luciano Lamberti, Italy  
Andreas Lampropoulos , United Kingdom  
Raffaele Landolfo, Italy  
Massimo Latour , Italy  
Bang Yeon Lee , Republic of Korea  
Eul-Bum Lee , Republic of Korea  
Zhen Lei , Canada  
Leonardo Leonetti , Italy  
Chun-Qing Li , Australia  
Dongsheng Li , China  
Gen Li, China  
Jiale Li , China  
Minghui Li, China  
Qingchao Li , China  
Shuang Yang Li , China  
Sunwei Li , Hong Kong  
Yajun Li , China  
Shun Liang , China  
Francesco Liguori , Italy  
Jae-Han Lim , Republic of Korea  
Jia-Rui Lin , China  
Kun Lin , China  
Shibin Lin, China

Tzu-Kang Lin , Taiwan  
Yu-Cheng Lin , Taiwan  
Hexu Liu, USA  
Jian Lin Liu , China  
Xiaoli Liu , China  
Xuemei Liu , Australia  
Zaobao Liu , China  
Zhuang-Zhuang Liu, China  
Diego Lopez-Garcia , Chile  
Cristiano Loss , Canada  
Lyan-Ywan Lu , Taiwan  
Jin Luo , USA  
Yanbin Luo , China  
Jianjun Ma , China  
Junwei Ma , China  
Tian-Shou Ma, China  
Zhongguo John Ma , USA  
Maria Macchiaroli, Italy  
Domenico Magisano, Italy  
Reza Mahinroosta, Australia  
Yann Malecot , France  
Prabhat Kumar Mandal , India  
John Mander, USA  
Iman Mansouri, Iran  
André Dias Martins, Portugal  
Domagoj Matesan , Croatia  
Jose Matos, Portugal  
Vasant Matsagar , India  
Claudio Mazzotti , Italy  
Ahmed Mebarki , France  
Gang Mei , China  
Kasim Mermerdas, Turkey  
Giovanni Minafò , Italy  
Masoomah Mirrashid , Iran  
Abbas Mohajerani , Australia  
Fadzli Mohamed Nazri , Malaysia  
Fabrizio Mollaioli , Italy  
Rosario Montuori , Italy  
H. Naderpour , Iran  
Hassan Nasir , Pakistan  
Hossein Nassiraei , Iran  
Satheeskumar Navaratnam , Australia  
Ignacio J. Navarro , Spain  
Ashish Kumar Nayak , India  
Behzad Nematollahi , Australia

Chayut Ngamkhanong , Thailand  
Trung Ngo, Australia  
Tengfei Nian, China  
Mehdi Nikoo , Canada  
Youjun Ning , China  
Olugbenga Timo Oladinrin , United Kingdom  
Oladimeji Benedict Olalusi, South Africa  
Timothy O. Olawumi , Hong Kong  
Alejandro Orfila , Spain  
Maurizio Orlando , Italy  
Siti Aminah Osman, Malaysia  
Walid Oueslati , Tunisia  
SUVASH PAUL , Bangladesh  
John-Paris Pantouvakis , Greece  
Fabrizio Paolacci , Italy  
Giuseppina Pappalardo , Italy  
Fulvio Parisi , Italy  
Dimitrios G. Pavlou , Norway  
Daniele Pellegrini , Italy  
Gatheeshgar Perampalam , United Kingdom  
Daniele Perrone , Italy  
Giuseppe Piccardo , Italy  
Vagelis Plevris , Qatar  
Andrea Pranno , Italy  
Adolfo Preciado , Mexico  
Chongchong Qi , China  
Yu Qian, USA  
Ying Qin , China  
Giuseppe Quaranta , Italy  
Krishanu ROY , New Zealand  
Vlastimir Radonjanin, Serbia  
Carlo Rainieri , Italy  
Rahul V. Ralegaonkar, India  
Raizal Saifulnaz Muhammad Rashid, Malaysia  
Alessandro Rasulo , Italy  
Chonghong Ren , China  
Qing-Xin Ren, China  
Dimitris Rizos , USA  
Geoffrey W. Rodgers , New Zealand  
Pier Paolo Rossi, Italy  
Nicola Ruggieri , Italy  
JUNLONG SHANG, Singapore

Nikhil Saboo, India  
Anna Saetta, Italy  
Juan Sagaseta , United Kingdom  
Timo Saksala, Finland  
Mostafa Salari, Canada  
Ginevra Salerno , Italy  
Evangelos J. Sapountzakis , Greece  
Vassilis Sarhosis , United Kingdom  
Navaratnarajah Sathiparan , Sri Lanka  
Fabrizio Scozzese , Italy  
Halil Sezen , USA  
Payam Shafigh , Malaysia  
M. Shahria Alam, Canada  
Yi Shan, China  
Hussein Sharaf, Iraq  
Mostafa Sharifzadeh, Australia  
Sanjay Kumar Shukla, Australia  
Amir Si Larbi , France  
Okan Sirin , Qatar  
Piotr Smarzewski , Poland  
Francesca Sollecito , Italy  
Rui Song , China  
Tian-Yi Song, Australia  
Flavio Stochino , Italy  
Mayank Sukhija , USA  
Piti Sukontasukkul , Thailand  
Jianping Sun, Singapore  
Xiao Sun , China  
T. Tafsirojjaman , Australia  
Fujiao Tang , China  
Patrick W.C. Tang , Australia  
Zhi Cheng Tang , China  
Weerachart Tangchirapat , Thailand  
Xiixin Tao, China  
Piergiorgio Tataranni , Italy  
Elisabete Teixeira , Portugal  
Jorge Iván Tobón , Colombia  
Jing-Zhong Tong, China  
Francesco Trentadue , Italy  
Antonello Troncone, Italy  
Majbah Uddin , USA  
Tariq Umar , United Kingdom  
Muahmmad Usman, United Kingdom  
Muhammad Usman , Pakistan  
Mucteba Uysal , Turkey



Ilaria Venanzi , Italy  
Castorina S. Vieira , Portugal  
Valeria Vignali , Italy  
Claudia Vitone , Italy  
Liwei WEN , China  
Chunfeng Wan , China  
Hua-Ping Wan, China  
Roman Wan-Wendner , Austria  
Chaohui Wang , China  
Hao Wang , USA  
Shiming Wang , China  
Wayne Yu Wang , United Kingdom  
Wen-Da Wang, China  
Xing Wang , China  
Xiuling Wang , China  
Zhenjun Wang , China  
Xin-Jiang Wei , China  
Tao Wen , China  
Weiping Wen , China  
Lei Weng , China  
Chao Wu , United Kingdom  
Jiangyu Wu, China  
Wangjie Wu , China  
Wenbing Wu , China  
Zhixing Xiao, China  
Gang Xu, China  
Jian Xu , China  
Panpan , China  
Rongchao Xu , China  
HE YONGLIANG, China  
Michael Yam, Hong Kong  
Hailu Yang , China  
Xu-Xu Yang , China  
Hui Yao , China  
Xinyu Ye , China  
Zhoujing Ye, China  
Gürol Yildirim , Turkey  
Dawei Yin , China  
Doo-Yeol Yoo , Republic of Korea  
Zhanping You , USA  
Afshar A. Yousefi , Iran  
Xinbao Yu , USA  
Dongdong Yuan , China  
Geun Y. Yun , Republic of Korea

Hyun-Do Yun , Republic of Korea  
Cemal YİĞİT , Turkey  
Paolo Zampieri, Italy  
Giulio Zani , Italy  
Mariano Angelo Zanini , Italy  
Zhixiong Zeng , Hong Kong  
Mustafa Zeybek, Turkey  
Henglong Zhang , China  
Jiupeng Zhang, China  
Tingting Zhang , China  
Zengping Zhang, China  
Zetian Zhang , China  
Zhigang Zhang , China  
Zhipeng Zhao , Japan  
Jun Zhao , China  
Annan Zhou , Australia  
Jia-wen Zhou , China  
Hai-Tao Zhu , China  
Peng Zhu , China  
QuanJie Zhu , China  
Wenjun Zhu , China  
Marco Zucca, Italy  
Haoran Zuo, Australia  
Junqing Zuo , China  
Robert Černý , Czech Republic  
Süleyman İpek , Turkey

## Contents


---

### **Analysis of Lightweight Polystyrene Foam Concrete Flat Slabs under Fire Condition**

Majed Alzara, Magdy Riad, Mohamed AbdelMongy, Mohamed A. Farouk, Ahmed M. Yosri , Ahmed M. Moubarak, and Ahmed Ehab

Research Article (11 pages), Article ID 1964903, Volume 2022 (2022)

### **Response of the Flat Reinforced Concrete Floor Slab with Openings under Cyclic In-Plane Loading**

Eden Shukri Kalib and Yohannes Werkina Shewalul 

Research Article (9 pages), Article ID 2503475, Volume 2021 (2021)



## Research Article

# Analysis of Lightweight Polystyrene Foam Concrete Flat Slabs under Fire Condition

**Majed Alzara,<sup>1</sup> Magdy Riad,<sup>2</sup> Mohamed AbdelMongy,<sup>1,3</sup> Mohamed A. Farouk,<sup>4</sup> Ahmed M. Yosri <sup>1,4</sup> Ahmed M. Moubarak,<sup>4</sup> and Ahmed Ehab<sup>5</sup>**

<sup>1</sup>Department of Civil Engineering, Jouf University, Sakakah, Saudi Arabia

<sup>2</sup>Civil Engineering Department, Higher Institute of Engineering, El Shourouk Academy, El Shourouk, Egypt

<sup>3</sup>Civil Engineering Department, Faculty of Engineering, Al-Azhar University, Cairo, Egypt

<sup>4</sup>Civil Engineering Department, Faculty of Engineering, Delta University for Science and Technology, Belkas, Egypt

<sup>5</sup>Department of Civil Engineering, Badr University in Cairo, Badr, Egypt

Correspondence should be addressed to Ahmed M. Yosri; [engineering@ju.edu.sa](mailto:engineering@ju.edu.sa)

Received 12 November 2021; Revised 8 May 2022; Accepted 21 May 2022; Published 22 June 2022

Academic Editor: Giovanni Garcea

Copyright © 2022 Majed Alzara et al. This is an open access article distributed under the Creative Commons Attribution License, which permits unrestricted use, distribution, and reproduction in any medium, provided the original work is properly cited.

Lightweight reinforced concrete (LWC) is widely used in various reinforced concrete (RC) applications, such as its use in diverse types of reinforced concrete slabs. The aim of this study is to analyze the behavior of reinforced foam concrete slabs (flat slab type) that are exposed to fire conditions under the influence of eccentric loads as well as concentric loads. This analysis has been done using the finite element method by a (ANSYS) software program. The validity of the adopted models was verified through comparison with a previous experimental study. The studied specimens were eleven reinforced concrete flat slabs with a thickness of 150 mm. The lightweight polystyrene foam concrete was used in these specimens with a density of 1820 kg/m<sup>3</sup>. The results showed that the fire effect lead to a decrease in the maximum carrying load of foam concrete slabs by 25%. Also, by comparing the finite element results with the selected experimental study, the results showed a great agreement with the analytical study used in this research.

## 1. Introduction

The use of lightweight concrete has been widespread since the 18th century. There was a necessary need to use this type of concrete to reduce the cost of reinforced concrete structures. Looking at the main factors that have effects on reducing the weight and density of concrete, the weight and type of the aggregate used as well as the ratio between coarse aggregate and fine aggregate are the main factors that can be used for this purpose.

It is also possible to use foam in its various forms in mixed concrete materials in order to produce the lightweight concrete. Numerous and varied studies have dealt with the use of foam in the production of lightweight concrete. Due to the availability of manufacturing foam of different types in many countries, it can be used in a simple way to produce this type of concrete. In 2014, M. Tech Scholar [1] have made

an analytical study of two mixtures of foam concrete, the first mixture of foam concrete with sand and the second mixture without sand, and the study dealt with many experiments to determine the proportions of the concrete mixture to reach a density of 1900 kg/m<sup>3</sup>. This study concluded that the ratio of the mixture which is used in the study is not suitable for the production of foam concrete which can be used in structural purposes because the compressive strength resulting from the concrete was less than 17.0 MPa, after 28 days of casting.

Helal et al. [2] conducted a practical study for the purpose of improving the preformed foam concrete, which was produced with a density of 1300 to 1900 kg/m<sup>3</sup>. This study relied on the use of two types of materials that are added to concrete (fly ash and silica fume) in addition to use of a water reducing agent. The results of this study were good, as these materials showed a clear improvement in the

structure of concrete pores, as well as an increase in strength, in addition to a reduction in concrete's absorption of water. The results also showed that these materials had slightly increased the thermal conductivity of concrete.

According to the study conducted by Wan Ibrahim et al. [3], the effect of polyolefin fibers on the properties of foam concrete was studied (such as flexural strength and compressive strength). The density of concrete that is used in this study ranged from 1300 to 1600 kg/m<sup>3</sup>. The researchers used in the study polyolefin sized fibers at relatively low volume fraction with percentages ranging from 0.0%, 0.20%, 0.40%, and 0.60%. The results of the study were that the compressive strength and flexural strength of foam concrete were slightly affected as a result of using the mentioned fibers by 4.3% and 9.3%, respectively.

Also, the researchers of Lee et al. (2017) [4] have conducted their study on slabs and beams of foam concrete, which was produced using a type of lightweight foam mortar, and the density of concrete ranged from 1700 to 1800 kg/m<sup>3</sup>. Accordingly, the concrete's compressive strength was 20 MPa. The results of this study were that the mortar used led to a decrease in the maximum load from 8.0% to 34.0%, when compared to that of reinforced concrete with natural density using the same type of mortar.

By reviewing the reviews and previous studies, it was found that foam concrete can be used successfully in reinforced concrete structures by using additives and different types of fibers. Concrete slabs made of structural polystyrene foam can be used to replace hollow block panels and thermally insulated layers.

Several design models were developed for punching shear strength; however, these models vary significantly in the considered parameters and mechanisms in developing the model [5–9]. For example, the European concrete design code (EC2) [5] model is semiempirical. In contrast, the FIB model design code (MC) [6] is physically based. Thus, there are many reviews that have studied the performance of flat slabs when exposed to fire. References [10–18]. Despite the diversity of these studies, it was noted that the behavior of polystyrene foam concrete when exposed to fire was not studied.

El-Fitiany and Youssef [13] in their study conducted a simple method to predict the flexural and behavior of reinforced concrete sections during exposure to high temperatures. This proposed method was validated experimentally by an analytical study. Wang [14] experimentally studied the structural behavior of reinforced foam concrete flat slab exposed to fire under diverse loading such as concentric and eccentric. The eleven flat slab specimens with square dimensions of 1750 mm length and 150 mm thickness were tested. The central column with a square cross section 200 × 200 mm was located at the center of each slab. The results in that study showed that the maximum load of the specimens with light weight foam concrete were reduced compared to those of specimens with normal concrete.

The main purpose of this study is to identify the efficiency of structural lightweight polystyrene foam concrete flat slabs under varies parameters when these slabs are exposed to fire.

## 2. Materials and Methods

The validity of the adopted models was verified through a comparison with a previous experimental study which was conducted by Riad and Shoeib [18]. In their study, two concrete mixes were used, one for the light weight concrete specimens and another mix was for the normal concrete specimens. Polystyrene foam, silica fume, and super plasticizer were used in the mix in order to achieve the self-compacting lightweight concrete; also, fine crushed stone of nominal maximum size of 10 mm was used as a coarse aggregate. Steel rebars with grades (240/350) and (360/520) were used. The yield strength and ultimate tensile strength for a mild steel (240/350) were (240 MPa) and (350 MPa), respectively, and this steel was 8 mm in diameter. The proof strength of high tensile steel deformed rebars with grade (360/520) was 360 MPa and ultimate tensile strength of these were 520 MPa. This rebars with bar sizes of (12 mm) and (16 mm).

## 3. Numerical Program

*3.1. Numerical Specimens and Parameters.* The numerical specimens included eleven tested RC simply supported square slabs with typical dimensions of 150 mm thickness and 1750 mm length. The clear span was equal to 1650 mm. The RC column is square with 200 mm in the case of the concentric load. In the case of an eccentric load, the column was extended above the slab compression face by 200 mm for all tested specimens. The typical concrete specimen's dimensions and reinforcement details are shown in Figure 1 as the experimental specimens that are presented by Riad and Shoeib [18].

The main parameters in this work are the effect of the percentage of tension steel reinforcement (0.40% and 0.70%) and type of vertical loads (concentric or eccentric) on the performance of flat slab when exposed to fire. Five specimens with normal-weight concrete and six specimens with polystyrene foam concrete slab have been tested.

The eleven tested specimens are divided into four groups as shown in Figure 2 and as follows:

- (i) The first group (3 control specimens) studies the behavior of normal-weight concrete with different load types and steel ratios.
- (ii) The second group (2 specimens) studies the behavior of normal-weight concrete exposed to fire from 0 to 500°C and is loaded by 30% of the ultimate with gradual increasing to ultimate load after cooling by air.
- (iii) The third group, (3 specimens), and considers the effect of the load type and main steel ratios on the behavior of lightweight concrete
- (iv) The fourth group (3 specimens) is similar to the second group but by using lightweight concrete instead of the normal concrete.

*3.2. Modeling Slabs by ANSYS.* This section presents elements types, real constant, material properties, numerical concepts, boundary conditions, and analysis types so as process together with load stepping.

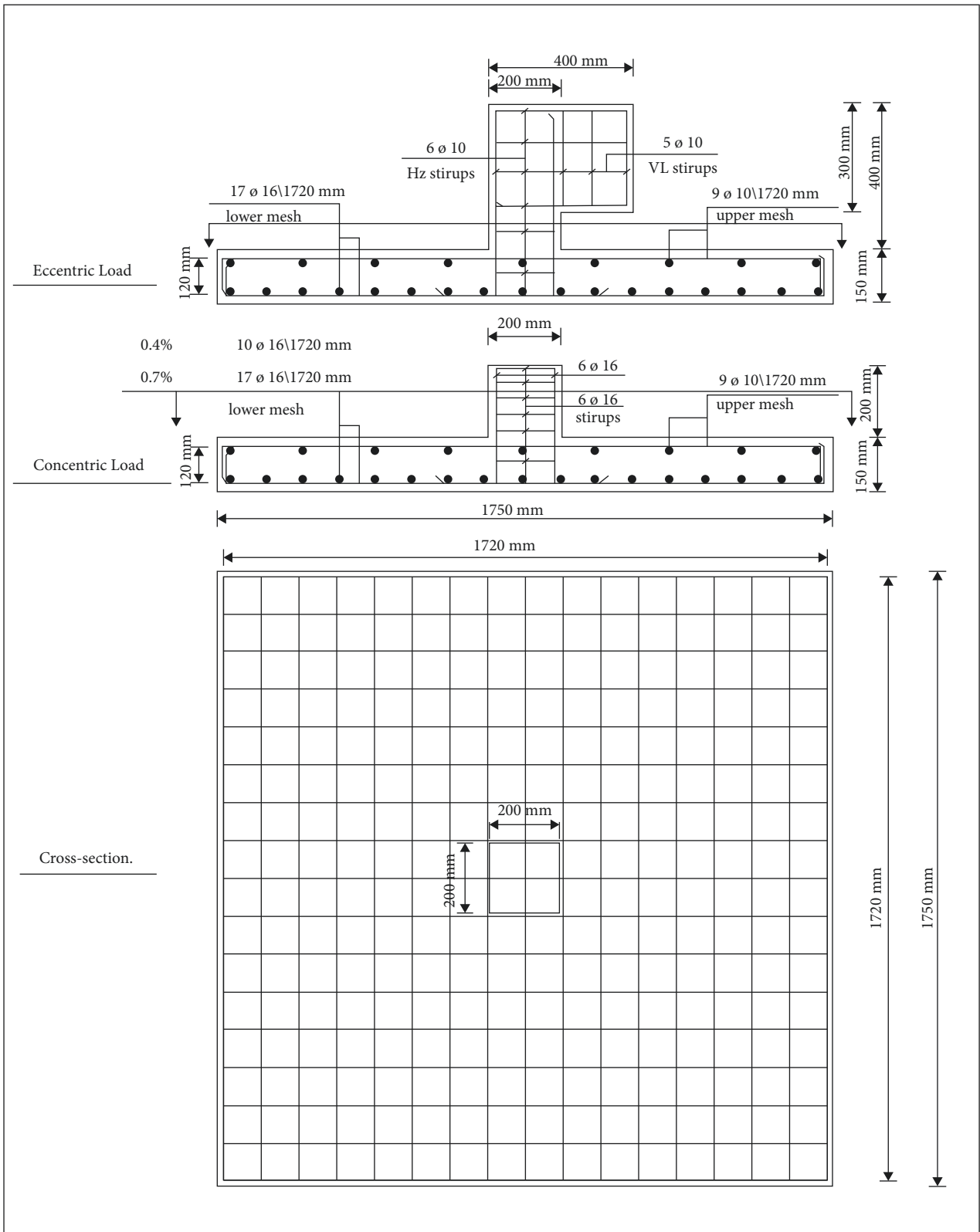


FIGURE 1: Typical dimensions and RFT for tested specimens.

3.2.1. *Elements Types.* There are mainly four elements used at the analysis; the names, shapes, number of degree of freedom, and some properties are shown below in Table 1.

3.2.2. *Loads and Boundary Conditions.* Similarly, for the experimental slabs, all joints at the border of the slab are modeled as a simply supported, which was constrained in the UY. Two nodes in the X direction are constrained in the



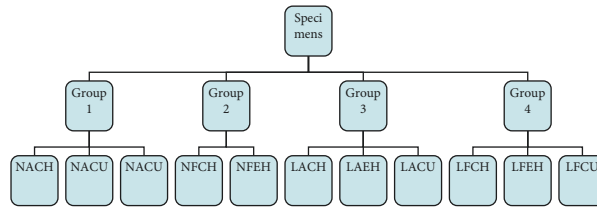


FIGURE 2: Main groups of specimens. *N*\* normal-weight concrete (NWC), *L*\* lightweight concrete (LWC), *A*\* without fire, *F*\* exposed to fire, *C*\* under concentric load, *E*\* under eccentric load, *U*\* 0.4% Rft (Reinforced steel ratio) from gross area of slab, and *H*\* 0.7% Rft from gross area of slab.

TABLE 1: Summary for the elements needed at modeling.

Properties\element	Concentric element		Steel reinforcement element	Lead Plate and Supports
Name	Solid65 (structural concentric element)	Solid75 (thermal concentric element)	Link180	Solid185
Shape				
No. of nodes	8	8	3	8
Properties	1-capable of plastic-deformation 2-cracking in 3-orthogonal direction 3-crushing	1-having thermal degree-of-freedom 2-using at heat condition	1-Proficient in plastic-deformation 2-connected between nodes 3-2 materials share the same nodes	1-Plastic and hyper-elastic 2-allows for stress-stiffening 3-creep so as large deflection together with large strain

*UX* and another two nodes, in the *Y* direction *UY*. The displacement is applied at the column head based on its position. The displacement is applied at a single node on upper plate using the incremental displacement method. The support and the displacement applied are presented in Figure 3.

#### 4. Verification of the Analytical Model

Table 2 shows the verification of the analytical model and experimental slabs which was tested by Riad and Shoeib [18]; the table divided into two main categories related to the output of the analysis. The first category shows the failure loads for each specimen at experimental and analytical models and the percentage of difference between both. The second category is the same but for the deflection at edge of column.

4.1. *Crack Patterns and Load-Deflection Curves.* Table 3 shows the propagation of cracks of the slabs specimen 1, 3, 6, and 8 just before failure using the finite element model and actual failure shape and load-deflection curves.

4.2. *Parametric Study and Effect of Eccentricity on the Behavior of a Flat Slab.* To study the effect of eccentricity on the behavior of lightweight concrete, the specimens are divided to four groups, each group includes eight specimens related to the ratios of steel (0.4 and 0.7 which are called *U* and *H*,

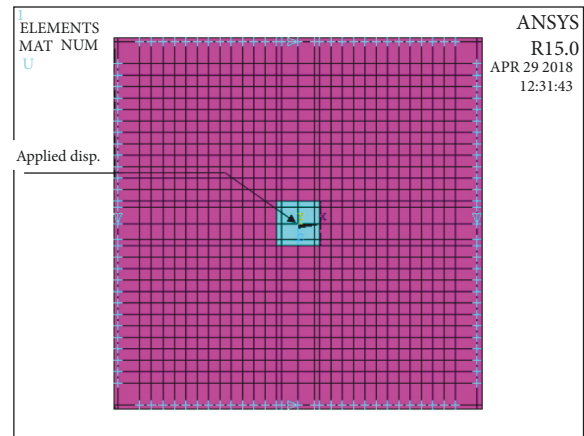


FIGURE 3: Support condition and applied displacement.

respectively), the eccentricity which varies from 0.5 to 1 with a 25% increasing fixed percentage, type of concrete, and heating intensity or temperature are as shown in the table below. Table 4 has been expressed as a database at the nonlinear finite element analysis for the same slab cross section and steel grade as the experimental program.

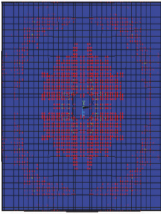
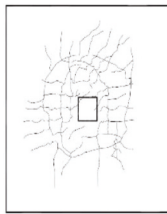
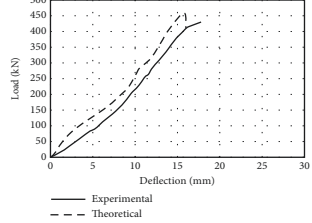
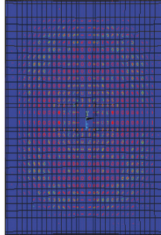

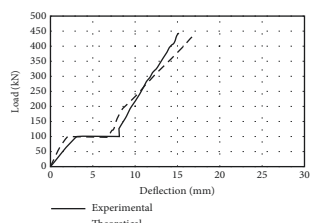
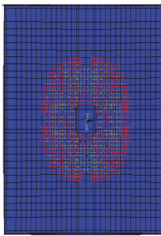

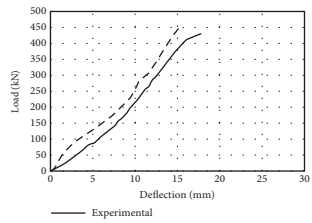
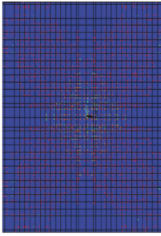

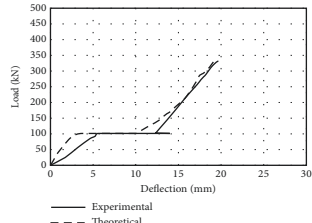
4.3. *Parametric Study Database Analysis and Results.* A nonlinear finite analysis is conducted using ANSYS software, to

TABLE 2: Verification of the analytical model and tested specimens of Riad and Shoeib [18].

Group	Specimen	Specimens code	Failure load (kN)			Deflection at edge of column (mm)		
			Experimental	Analytical	% diff.	Experimental	Analytical	% diff.
G1	S1	NACH	462	483.7	4.7	13.92	13.4	-3.74
	S2	NAEH	382	417.6	9.3	12.3	11.65	-5.28
	S5	NACU	383	396.95	3.64	15.1	14.67	-2.85
G2	S3	NFCH	444	451.23	1.65	15.15	17.43	15.0
	S4	NFEH	298.7	311.73	4.36	15	14.85	-1.0
G3	S6	LACH	430	459.7	6.9	17.72	16.04	-9.48
	S7	LAEH	367	406.4	10.73	11.4	12.28	7.71
	S11	LACU	343	376.6	9.8	15.5	14.55	-6.13
G4	S8	LFCH	332	341.33	3	19.75	19.44	-1.57
	S9	LFEH	238	272.24	14.38	14.33	13.23	-7.68
	S10	LFCU	278	286.7	3.13	15.9	15.95	0.5

2. *N* \* normal-weight concrete, *L* \* lightweight concrete, *A* \* without fire, *F* \* exposed to fire, *C* \* under concentric load, *E* \* under eccentric load, *U* \* 0.4% rft from gross area of slab, *H* \* 0.7% rft from gross area of slab.

TABLE 3: Summary of finite element models, cracks, and load-deflection curves.

Sample	Finite element model	Crack	Load-deflection
S1 (NACH)			
S3 (NFCH)			
S6 (LACH)			
S8 (LFCH)			

predict the ultimate loads and deflection for the constructed parametric study database. The finite element predicted failure loads and deflection at edge of column. Figure 4 presents the crack propagation before ultimate from the finite element model.

In case of the study of the behavior of lightweight RC, flat slabs with RFT percentages equal to 0.7% and 0.4% when applying the concentric and changing eccentric vertical load  $e/t = 0.5, 0.75$  and  $1.0$ .

TABLE 4: Parametric study database of slabs.

Group	Specimens	Specimens code	Type of concrete	Heating temp (C°)	Eccentricity ratio ( $e/t$ )	Main RFT%	Flexure RFT
G1	1	NACH	NWC	Non	No	H	17 Ø 16
	2	NAE <sub>1</sub> H			0.5		17 Ø 16
	3	NAE <sub>2</sub> H			0.75		17 Ø 16
	4	NAE <sub>3</sub> H			1.0		17 Ø 16
	5	NACU			No	U	10 Ø 16
	6	NAE <sub>1</sub> U			0.5		10 Ø 16
	7	NAE <sub>2</sub> U			0.75		10 Ø 16
	8	NAE <sub>3</sub> U			1.0		10 Ø 16
G2	9	NFCH	NWC	500°	No	H	17 Ø 16
	10	NFE <sub>1</sub> H			0.5		17 Ø 16
	11	NFE <sub>2</sub> H			0.75		17 Ø 16
	12	NFE <sub>3</sub> H			1.0		17 Ø 16
	13	NFCU			No	U	10 Ø 16
	14	NFE <sub>1</sub> U			0.5		10 Ø 16
	15	NFE <sub>2</sub> U			0.75		10 Ø 16
	16	NFE <sub>3</sub> U			1.0		10 Ø 16
G3	17	LACH	LWC	Non	No	H	17 Ø 16
	18	LAE <sub>1</sub> H			0.5		17 Ø 16
	19	LAE <sub>2</sub> H			0.75		17 Ø 16
	20	LAE <sub>3</sub> H			1.0		17 Ø 16
	21	LACU			No	U	10 Ø 16
	22	LAE <sub>1</sub> U			0.5		10 Ø 16
	23	LAE <sub>2</sub> U			0.75		10 Ø 16
	24	LAE <sub>3</sub> U			1.0		10 Ø 16
G4	25	LFCH	LWC	500°	No	H	17 Ø 16
	26	LFE <sub>1</sub> H			0.5		17 Ø 16
	27	LFE <sub>2</sub> H			0.75		17 Ø 16
	28	LFE <sub>3</sub> H			1.0		17 Ø 16
	29	LFCU			No	U	10 Ø 16
	30	LFE <sub>1</sub> U			0.5		10 Ø 16
	31	LFE <sub>2</sub> U			0.75		10 Ø 16
	32	LFE <sub>3</sub> U			1.0		10 Ø 16

N \* normal-weight concrete, L \* lightweight concrete, A \* without fire, F \* exposed to fire, C \* under concentric load, E<sub>1</sub> \*, E<sub>2</sub> \* and E<sub>3</sub> \* under eccentric load ( $e/t$ ) = 0.5, 0.75 and 1.0 respectively, U \* 0.4% rft from gross area of slab, H \* 0.7% rft from gross area of slab.

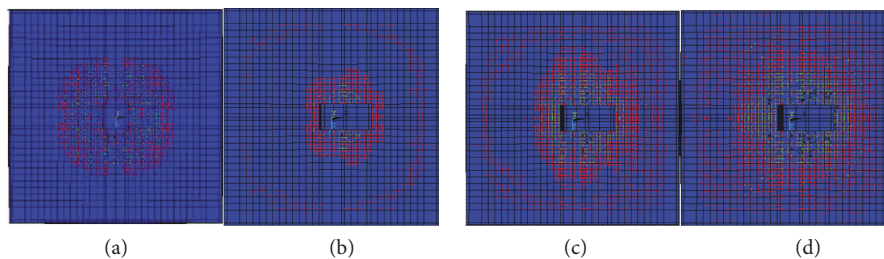


FIGURE 4: Crack propagation before failure from the finite element model. (a)  $e/t=0$ . (b)  $e/t=0.5$ . (c)  $e/t=0.75$ . (d)  $e/t=1.0$ .

In case of high RFT percentage equal to 0.7%, the effect of applying the concentric and the changing eccentric vertical load LAE<sub>1</sub>H, LAE<sub>2</sub>H and LAE<sub>3</sub>H with  $e/t = 0.5, 0.75$ , and  $1.0$ , respectively, on the behavior of lightweight RC flat slabs was noted as the following.

It is clear from Figures 5 and 6, when applying the eccentric vertical load LAE<sub>1</sub>H, LAE<sub>2</sub>H, and LAE<sub>3</sub>H with  $e/t = 0.5, 0.75$ , and  $1.0$ , respectively, on the tested specimens with high RFT% that the ultimate load decreased compared to a concentric control specimen (LACH) by percentage 11.59%, 30.19%, and 44.15%, respectively, and the deflection

corresponding to the ultimate load decreased with percentage 23.44%, 28.43% and 34.16%, respectively. It is also noted that the stiffness of these tested specimens increased by increasing the eccentric vertical load, although the stiffness of the eccentric specimen with  $e/t = 1.0$  becomes similar to concentric control specimen, as shown in Figure 5.

In case of usual RFT percentage equals to 0.4%, the effect of applying the concentric and the changing eccentric vertical load LAE<sub>1</sub>U, LAE<sub>2</sub>U, and LAE<sub>3</sub>U with  $e/t = 0.5, 0.75$ , and  $1.0$ , respectively, on the behavior of a lightweight RC flat slab was noted as shown in figures 5 to 8.

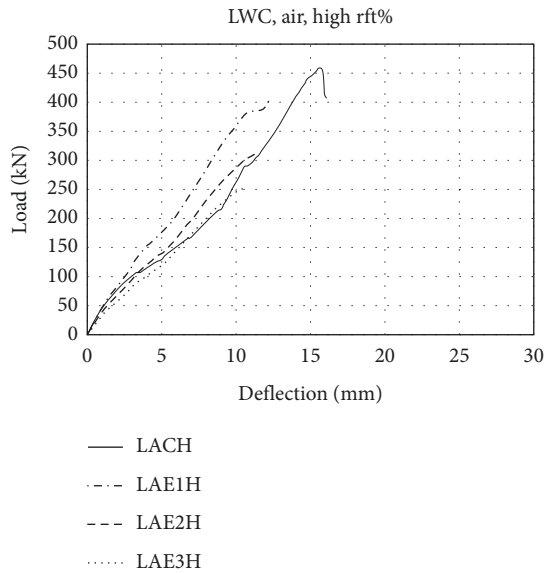


FIGURE 5: Effect of  $e/t$  ratio on the load-deflection curves for LWC with high RFT%.

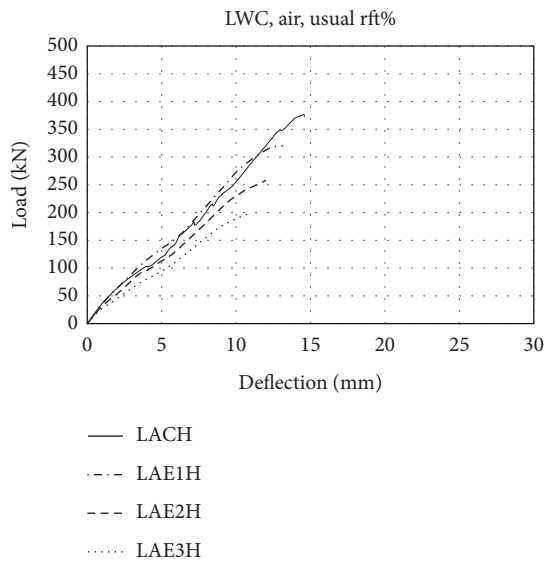


FIGURE 6: Effect of  $e/t$  ratio on the load-deflection curves for LWC with usual RFT%.

It is clear from Figures 7 and 8, when applying the eccentric vertical load LAE<sub>1</sub>U, LAE<sub>2</sub>U, and LAE<sub>3</sub>U with  $e/t = 0.5, 0.75,$  and  $1.0,$  respectively, on the tested specimens with usual RFT% that the ultimate load decreased compared to concentric control specimen (LACU) by percentage 15.10%, 31.40%, and 47.27%, respectively, and the deflection corresponding to the ultimate load decreased with percentage 10.65%, 17.73%, and 24.74%, respectively. It is also noted that the stiffness of these tested specimens increased by increasing the eccentric vertical load, although the eccentric specimen with  $e/t = 0.5$  have the same stiffness of concentric control specimen as shown in Figure 7.

On studying the behavior of lightweight RC, flat slabs which had been exposed to fire with RFT percentages equal

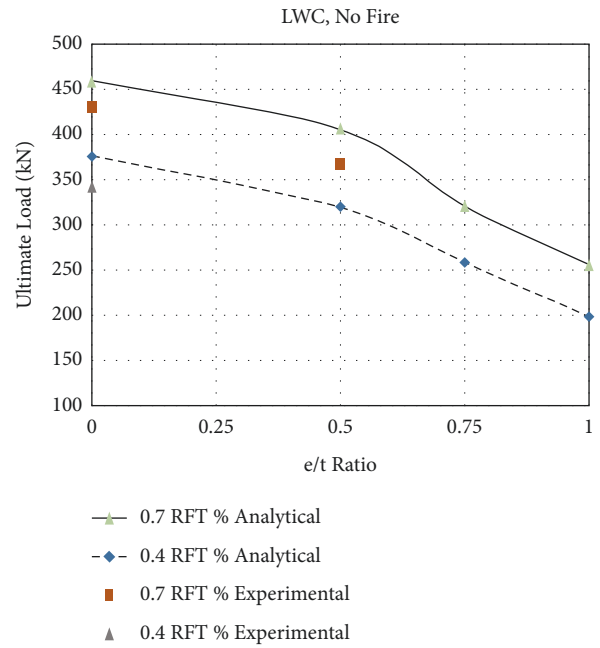


FIGURE 7: Effect of  $e/t$  ratio on load for LWC the ultimate.

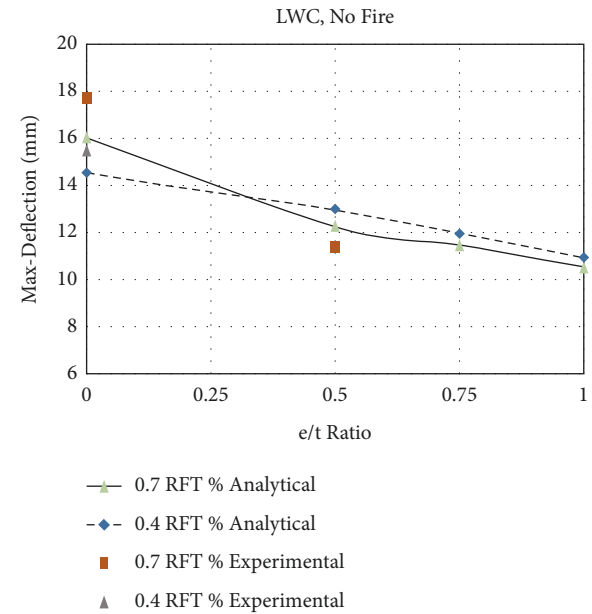


FIGURE 8: Effect of  $e/t$  ratio on the maximum deflection for LWC.

to 0.7% and 0.4% when applying the concentric and changing eccentric vertical load  $e/t = 0.5, 0.75$  and  $1.0.$

4.3.1. Discussion for Specimens with High RFT Percentage Equal to 0.7%,  $e/t$  (0 to 1) and Exposed to Fire. Figures 9 and 10 illustrate that when applying the eccentric vertical load LFE<sub>1</sub>H, LFE<sub>2</sub>H, and LFE<sub>3</sub>H with  $e/t = 0.5, 0.75,$  and  $1.0,$  respectively, on the tested specimens were exposed to fire with high RFT% that the ultimate load decreased comparing to concentric control specimen (LFCH) by percentage 20.24%, 44.10%, and 61.58%, respectively. The corresponding deflection to the ultimate load decreases with

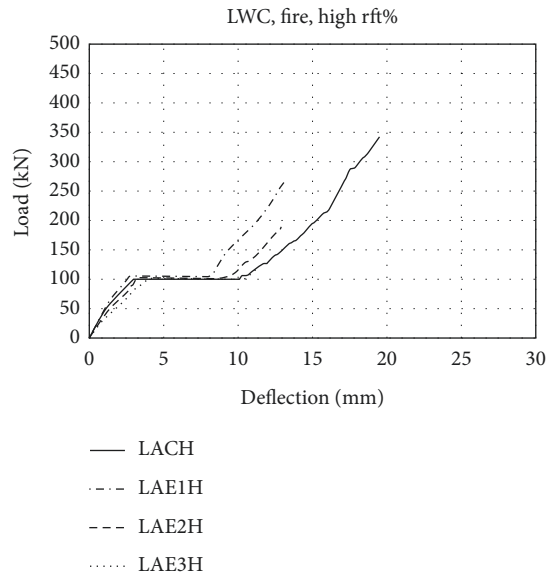


FIGURE 9: Effect of  $e/t$  ratio on the load-deflection curves for LWC with high RFT% when exposed to fire.

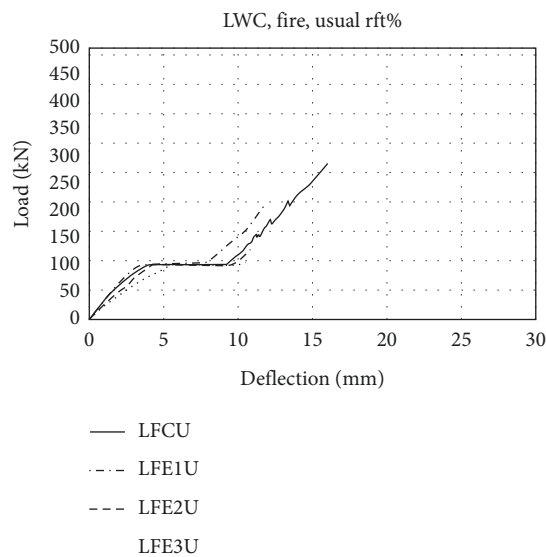


FIGURE 10: Effect of  $e/t$  ratio on the load-deflection curves for LWC with usual RFT% when exposed to fire.

percentage 31.94%, 33.28%, and 38.58%, respectively. The stiffness of those tested specimens increased by increasing the eccentricity, although the stiffness of the eccentric specimen with  $e/t=1.0$  becomes similar to concentric control specimen as shown in Figure 9.

**4.3.2. Discussion for Specimens with Usual RFT Percentage Equal to 0.4%,  $e/t$  (0 to 1) and Exposed to Fire.** Figures 9 and 10 illustrate that the applying eccentric vertical load LFE<sub>1</sub>U, LFE<sub>2</sub>U, and LFE<sub>3</sub>U with  $e/t=0.5, 0.75,$  and  $1.0,$  respectively, on the tested specimens which exposed to fire with usual

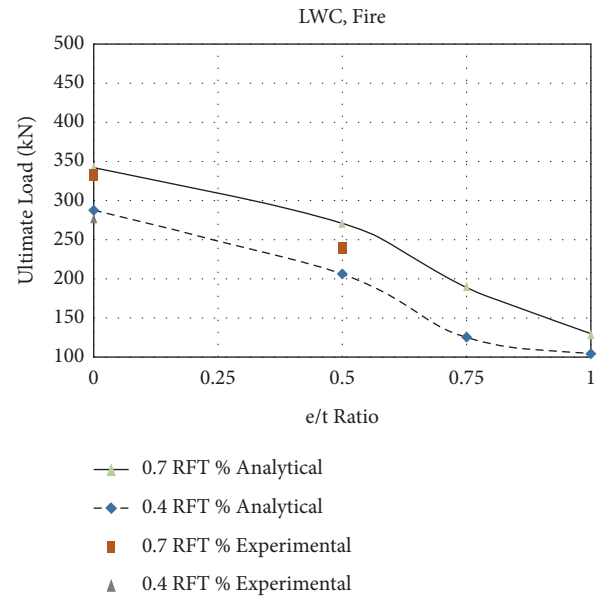


FIGURE 11: Effect of  $e/t$  ratio on the ultimate load for LWC when exposed to fire.

RFT% that will cause a decreasing in the ultimate load when comparing it to the concentric control specimen (LFCU) by percentage 27.76%, 55.94%, and 63.20%, respectively. Also, the corresponding deflection to the ultimate load decreases with percentage 26.96%, 32.79%, and 34.29%, respectively.

The stiffness of these tested specimens will be increased by increasing the eccentric vertical load, although the eccentric specimen with  $e/t=0.5$  have the same stiffness of concentric control specimen as shown in Figures 11 and 12.

For more clarification, Figure 13 presents the relation between variation of eccentricity( $e/t$ ) and deflection during the fire process with a constant load for LWC specimens at high and usual RFT% (0.7% and 0.4%, respectively). Related to the control specimen (LFCH), the deflection of high RFT% decreased by approximately 16.5%. Similarly for control specimen (LFCU), the deflection of usual RFT% decreased by approximately 13.3%.

## 5. Comparison of Parametric Study Database- Ultimate Loads and Loads from Different Codes Using the Proposal Factors for ACI 318 and BS 8110

Related to the experimental tests, reduction factors of concrete compressive strength in foam concrete depending on the reduction factors in lightweight concrete strength have been proposed by Riad and Shoeib [18]. In addition to, reduction factors in compressive strength of lightweight concrete exposed to 500°C fire for ACI-318 and BS-8110 codes were also proposed. This part discusses the comparison between the results of the finite element analysis, experimental tests, and different codes (ACI 318 and BS 8110) related to the mentioned reduction factors.



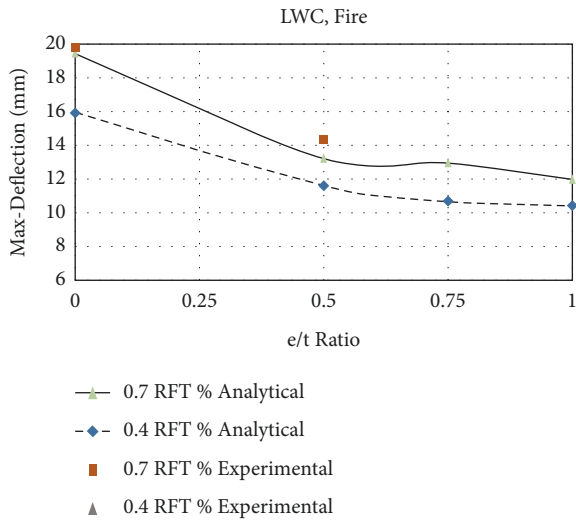


FIGURE 12: Effect of  $e/t$  ratio on the maximum deflection for LWC when exposed to fire.

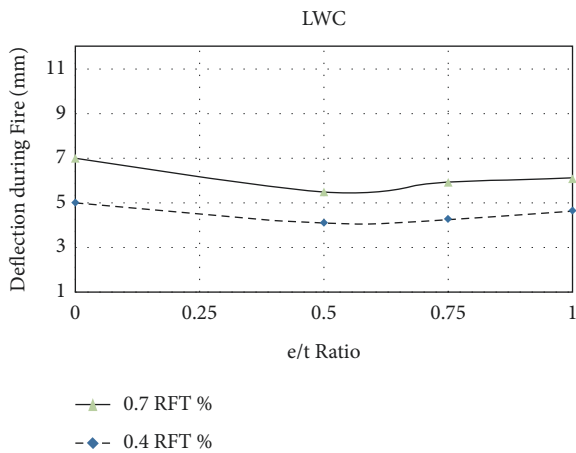


FIGURE 13: Effect of  $e/t$  ratio on the deflection during fire process at constant load for LWC.

Figure 14 appears in case LWC specimens were not exposed to fire by using the proposal reduction factors for ACI-318 and BS-8110 codes, the prediction load closes to database-ultimate loads by average percentage 24.0% and 16.25%, respectively, compared to the load using the reduction factors of these codes when increased  $e/t$  ratio to 0.5, 0.75, and 1.0. Figure 15 shows the comparison between the fired LWC database-ultimate loads and different codes which using the proposal factors.

Moreover, in case of LWC specimens that were exposed to fire, by using the proposal reduction factors for ACI-318 and BS-8110 codes, the prediction load closed to database-ultimate loads by an average percentage of 18.6% and 12.4%, respectively, compared to the load using the reduction factors of these codes when increased  $e/t$  ratio to 0.5, 0.75, and 1.0 as shown before in Figures 5–8.

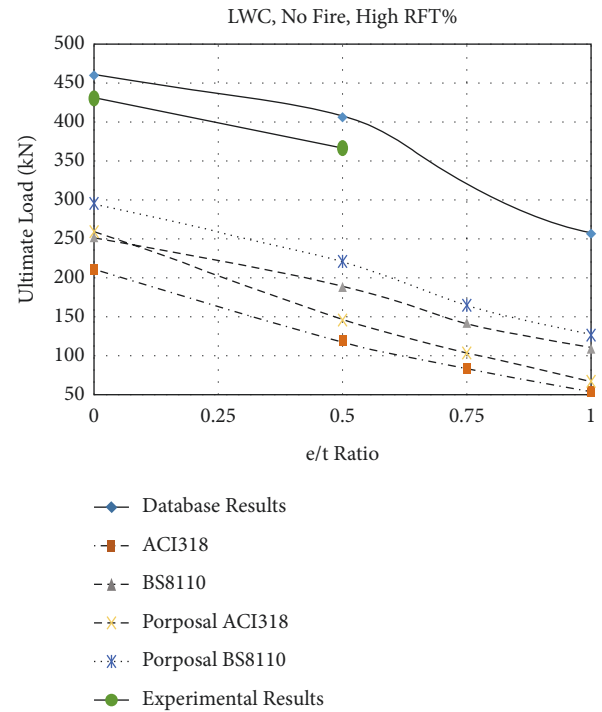


FIGURE 14: Comparison of LWC database-ultimate loads and different codes using the proposal factors.

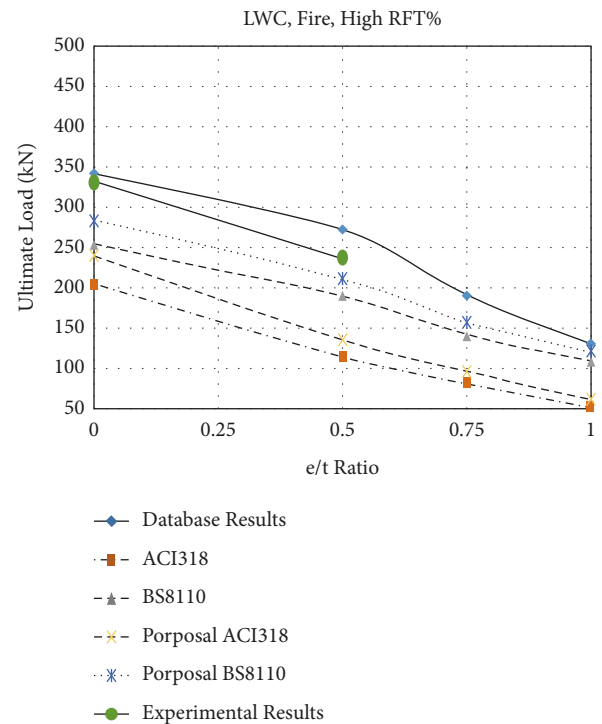


FIGURE 15: Comparison of fired LWC database-ultimate loads and different codes using the proposal factors.

## 6. Conclusion

The main purpose of this study is to identify the efficiency of structural lightweight polystyrene foam concrete flat slabs when these slabs are exposed to fire by the finite element

method. In this study, reinforced foam concrete flat slabs were exposed to fire under eccentric and concentric loads. The validity of the adopted models was verified through comparison with a previous experimental study which has been conducted by Riad and Shoeib [18]. By using the software analysis (ANSYS), crack patterns, load-deflection curves, steel strains, and deflection during the fire were analyzed in this study. The following are concluded in this work:

- (1) The density of lightweight structural concrete that was produced using fibers and additives was 1820 kg/m<sup>3</sup>, and the compressive strength of concrete reached 30.0 MPa.
- (2) When comparing the behavior of lightweight structural flat slabs which manufactured using polystyrene foam with that of normal-weight concrete flat slabs, we found the following:
  - (i) The maximum load was low in the lightweight foam concrete slab with rates ranging from 7.0% to 4% for concentric load and eccentric load, respectively; this is compared to the maximum load of normal-weight concrete.
  - (ii) A decrease in the number of cracks in lightweight foam concrete as well as an increase in the width of cracks was observed.
  - (iii) When calculating the theoretical punching shear force in ACI-318 and BS-8110 codes, the proposed modification factors of foam concrete can be equal to 1.24 and 1.163, respectively.
- (3) By comparing the behavior of the structural lightweight polystyrene foam concrete flat slab and normal-weight concrete flat slab exposed to fire, we find that:
  - (i) A decrease in the maximum load of foam concrete and normal-weight concrete was observed by 25% and 13%, respectively.
  - (ii) The recommended reduction factors in compressive strength according to ACI-318 and BS-8110 codes are 0.68 and 0.56 instead to 0.82 and 0.70, respectively.
- (4) It is highly recommended to study more specimens with different types of foams and fibers.

### Data Availability

The data used to support the findings of this study are included within the article and are available from the corresponding authors on reasonable request.

### Conflicts of Interest

The authors declare that they have no conflicts of interest.

### Authors' Contributions

Dr Ahmed Ehab and Dr Magdy Riad collected the data, conceived, and designed the analysis. Dr Ahmed. M. Yosri, Dr Mohamed Farouk, Dr. Mohamed Abdelmongy, and Dr Majed Alzara have performed the analyses, validated, discussed the results, and wrote the paper. All authors discussed the results and contributed to the final manuscript.

### References

- [1] M. Tech Scholar, "Experimental study on foam concrete," *International Journal of Civil, Structural, Environmental and Infrastructure Engineering Research and Development*, vol. 4, no. 1, pp. 145–158, 2014.
- [2] A. A. Hilal, N. H. Thom, and A. R. Dawson, *Foamed Concrete: From Weakness to Strength, 34th Cement and Concrete Science Conference*, University of Sheffield, Sheffield, UK, 2014.
- [3] M. H. Wan Ibrahim, N. Jamaluddin, J. M. Irwan, P. J. Ramadhansyah, and A. Suraya Hani, "Compressive and flexural strength of foamed concrete containing polyolefin fibers," *Advanced Materials Research*, vol. 91 I, pp. 489–493, 2014.
- [4] Y. Lee, H. Limjee, S. K. Lim, and C. S. Tan, "Flexural Behavior of Reinforced Lightweight Foamed Mortar Beams and Slab," *KSCE Journal of Civil Engineering*, pp. 1817–1822, 2017.
- [5] EN 1992-1-1, "Eurocode 2: design of concrete structures—Part 1–1: general rules and rules for buildings," British Standard Institution, London, UK, Incl. Corrigendum 1: EN 1992-1-1:2004/AC:2008, 2014.
- [6] B. Fédération Internationale Du, *Fib Model Code for Concrete Structures 2010*, Fédération Internationale Du Béton, Lausanne, Switzerland, 2013.
- [7] ACI-318-19, "ACI Committee 318; Building Code Requirements for Structural Concrete (ACI 318-19) and Commentary on Building Code Requirements (ACI 318-19)," American Concrete Institute: Farmington Hills, MI, USA, ACI-318-19, 2019.
- [8] ACI-318, "Building Code Requirements for Structural concrete (ACI 318) and Commentary ACI -318R," ACI-318, p. 369, American Concrete Institute, MI, USA, 2008.
- [9] BS-8110, "British Standard of Structural Use of concrete - Part 2: Code of Practice for Special Circumstances," Board of BSI, London, UK, BS-8110-2, 2005.
- [10] J. Hulimka, K. Rafał, and J. Agnieszka, "Laboratory Tests of Foam concrete Slabs Reinforced with Composite Grid," *Elsevier, Procedia Engineering*, pp. 337–344, 2017.
- [11] S. J. George, "Structural Performance of Reinforced Concrete Flat Plat Buildings Subjected to Fire," UNLV Theses, Dissertations, Professional Papers, and Capstones, Nevada, Las Vegas, 2012.
- [12] O. Kalmykov, "Study of fire-resistance of reinforced concrete slab of a new type," *MATEC Web of Conferences*, vol. 116, 2017.
- [13] S. F. El-Fitany and M. A. Youssef, "Assessing the flexural and axial behavior of reinforced concrete members at elevated temperatures using sectional analysis," *Fire Safety Journal*, vol. 44, pp. 691–703, 2009.

- [14] G. Wang, *Performance of Reinforced concrete Flat Slabs Exposed to Fire*, Master of Engineering, University of Canterbury, Christchurch, New Zealand, University of Canterbury, 2004 .
- [15] B. Wang, Y. Dong, and L. Gao, "Fire Experimental Study of Four-Edge Fixed Reinforced concrete Slab in Fire," *Advanced Materials Research*, vol. 163–167, 2011.
- [16] P. J. Moss, R. P. Dhakal, G. Wang, and A. H. Buchanan, "The fire behaviour of 17. multi-bay, two-way reinforced concrete slabs. *Engineering Structures*," vol. 30, no. 12, 2008.
- [17] I. A. Fletcher, S. Welch, J. L. Torero, and A. Usmani, "Behavior of concrete structures in fire," *Thermal Science*, vol. 11, no. 2, pp. 37–52, 2007.
- [18] M. Riad and S. Ata El-kareim Shoeib, "Behavior of structural lightweight polystyrene foam concrete flat slabs when exposed to fire," *The Open Construction & Building Technology Journal*, 2018.

## Research Article

# Response of the Flat Reinforced Concrete Floor Slab with Openings under Cyclic In-Plane Loading

Eden Shukri Kalib and Yohannes Werkina Shewalul 

*Faculty of Civil and Environmental Engineering, Jimma Institute of Technology, Jimma University, Jimma, Ethiopia*

Correspondence should be addressed to Yohannes Werkina Shewalul; [yesoro.work@gmail.com](mailto:yesoro.work@gmail.com)

Received 4 August 2021; Accepted 17 September 2021; Published 24 September 2021

Academic Editor: Giovanni Garcea

Copyright © 2021 Eden Shukri Kalib and Yohannes Werkina Shewalul. This is an open access article distributed under the Creative Commons Attribution License, which permits unrestricted use, distribution, and reproduction in any medium, provided the original work is properly cited.

The responses of flat reinforced concrete (RC) floor slabs with openings subjected to horizontal in-plane cyclic loads in addition to vertical service loads were investigated using nonlinear finite element analysis (FEA). A finite element model (FEM) was designed to perform a parametric analysis. The effects of opening sizes (7%, 14%, 25%, and 30% of the total area of the slab), opening shapes (elliptical, circular, L-shaped, T-shaped, cross, and rectangular), and location on the hysteretic behavior of the floor slab were considered. The research indicated that openings in RC floor slabs reduce the energy absorption capacity and stiffness of the floor slab. The inclusion of 30% opening on the floor slab causes a 68.5%, 47.3%, and 45.6% drop in lateral load capacity, stiffness, and lateral displacement, respectively, compared to the floor slab with no openings. The flat RC floor slab with a circular opening shape has increased efficiency. The placement of the openings is more desirable by positioning the openings at the intersection of two-column strips.

## 1. Introduction

As a primary horizontal structural element of building structures, the floor slab is susceptible to loads in and out of a plane, which are mostly attributable to lateral loads [1, 2]. It is therefore important to consider the combined effect of in-plane and out-of-plane loads when designing a slab of concrete for a building. It resists vertical forces for most of its design life. However, the floor structure can withstand horizontal seismic stresses during an earthquake that could last only between 10 and 100 seconds. It is termed a diaphragm during this brief period when the floor structure must withstand both gravity and horizontal forces [1].

The performance of the diaphragm action of the floor slab is controlled primarily by its in-plane stiffness. The floor diaphragm is considered rigid if it translates only on a plane and rotates as a rigid body about the vertical axis, whereas a flexible diaphragm is one in which the lateral force distribution to vertical lateral load resisting elements is depending on the tributary area. Finally, a stiff diaphragm is one that behaves in between the two [3–5]. An experimental and

analytical investigation was carried out at Lehigh University [6] to identify in-plane seismic behavior of floor diaphragm with scaled models representing a portion of a floor system in a building structure with various loading and support conditions. The diaphragm forces were applied in the plane of the floor system, both monotonically and cyclically. The hysteresis behavior was identified after the floor slab system experienced inelastic deformation.

In many structures, a reasonable estimate of the inertial force distribution can be achieved by assuming that the slabs act as a rigid diaphragm, but for structures with large openings and with noncompact shapes, diaphragm deformation of the floors must be explicitly considered in the analysis. Many building codes, including Euro code and ACI, have stated that failing to account for floor diaphragm flexibility when estimating the seismic response of floor diaphragms with large openings and noncompact or highly elongated in-plane shapes can lead to errors.

The effect of openings on the seismic capacity of floor diaphragm has been investigated by several researchers, and it has been confirmed that the presence of openings on the

floor diaphragm results in a substantial decrease in load capacity of the floor diaphragm. Previous research has indicated that the inelastic seismic response of the RC floor diaphragm is highly affected by the presence of openings, especially when cracking and yielding in the floor system. A micro FEM approach was used to identify the effect of opening size and out-of-plane loading on the inelastic seismic behavior of beam-supported floor diaphragm with the opening [7]. Openings or reentrant corners in the diaphragm must be properly placed and adequately reinforced [8].

In building, damage due to earthquake generally initiates at locations of structural weakness, and these weaknesses are mostly found at discontinuities in mass, stiffness, and strength of vertical and horizontal lateral load resisting elements. Nowadays because of architectural aesthetics and ventilation, floor slabs with openings have been used in many building structures. Besides building services, including stairways, elevators, air ducts, and pipes also need to pass through floor slabs, and in this process, there is weakness induced in the floor slab. Since it is necessary to understand the behavior of floor slabs with openings, different analytical studies based on experimental tests were conducted. But still, there is limited knowledge on the characteristics of RC floor slabs with different locations, shapes, and sizes of openings.

In the present study, flat RC floor slabs responses with different opening sizes, opening shapes, and locations of the openings under horizontal direct cyclic loading and vertical service loads were addressed utilizing an FEM approach. An FEA software, Abaqus/CAE, conducted the modeling and analysis to account for in-plane deformation and ultimate load capacity due to displacement-based cyclic load similar to that of the experimental investigation conducted in Lehigh University.

## 2. Finite Element Analysis of the Flat RC Floor Slab

The present study used the finite element approach to gather the relevant data regarding the behavior of floor diaphragms with openings using FEA, the Abaqus/CAE software. To check whether the simulation results reflect the real-world results, the flat floor slabs tested at Lehigh University in 1986 [6] were used for validation. The behavior of materials, support conditions, and loading procedures used in the experimental study by [6] was applied in the FEM. After the validation of the FEM, parametric study and sensitivity analysis were carried out by taking opening size, location, shape, service load, steel grade, and concrete grade as a parameter.

**2.1. Concrete Element Types.** In the present study, C3D8 (linear 8-node hexahedral brick elements) was used for modeling concrete material.

**2.2. Reinforcement Bars.** For elastic design analysis, the reinforcement was usually neglected in the FEM since the

stiffness contribution of concrete is much greater than the reinforcement, but in the nonlinear analysis, the modeling of reinforcement is needed basically in determining the ultimate capacity of a structure. The reinforcing bars were modeled as beam elements that are one-dimensional line elements in three-dimensional space that have stiffness associated with deformation in the line. Both elastic and plastic properties were included in the elastic option used to assign the modulus of elasticity and Poisson's ratio, and in the plastic option, the true stress and strain values were used to model its plastic property. Table 1 shows the mechanical properties of reinforcing bars that were used in the simulation that was taken from the experimental study conducted by [6].

**2.3. Concrete Constitutive Model.** Concrete exhibits non-linearity both in compression and tension; this poses difficulties in numerical analysis. Parameters needed to model concrete under compound stress were included in Abaqus/CAE software in the concrete damaged plasticity (CDP) model. One of the strength hypotheses most often applied to concrete is the Drucker-Prager hypothesis. On the basis of nondilatational strain energy, failure is defined by a cone-shaped boundary surface. The advantage of using this criterion is surface smoothness and thereby no complications in the numerical application. The drawback is that it is not fully consistent with the actual behavior of concrete [9]. The CDP model used in Abaqus/CAE software is a modification of the Drucker-Prager strength hypothesis. The CDP model parameters for uniaxial compression relations (Table 2) were adopted from the methods discussed by [10].

The tensile behavior of concrete utilized the bilinear model (Figure 1). The cracking opening was utilized instead of the tensile strain and was computed as a ratio of the total energy supplied ( $G_F$ ) per unit area required to create a crack in the concrete. Thus, the brittle behavior of concrete is defined by stress-cracking displacement rather than a stress-strain response [9].

Several complicated degradation mechanisms occur under uniaxial cyclic loading circumstances. Microcracks develop, close, and interact with each other. During uniaxial cyclic testing, it is noticed that the elastic stiffness recovers a little when the load changes sign. An essential element of concrete behavior under cyclic loading is the influence of stiffness recovery on the concrete's stiffness. As the load changes from tension to compression, the effect is generally more apparent, causing tensile cracks to close, resulting in the recovery of compressive stress [11].

The concrete damaged plasticity model supposes that the reduction of the elastic modulus is expressed in terms of a scalar degradation variable ( $d$ ) as in the following equation [11]:

$$E = (1 - d)E_o, \quad (1)$$

where  $E_o$  is the initial (undamaged) modulus of elasticity.

In Abaqus/CAE, default values of stiffness recovery factors  $w_t = 0$  and  $w_c = 1$  were used to illustrate the uniaxial load cycle behavior of concrete. In the present study, all

TABLE 1: The mechanical property of reinforcement bars.

Name	Area (mm <sup>2</sup> )	Yield stress (MPa)	Yield strain	Ultimate stress (MPa)	Ultimate strain	Modulus of elasticity (GPa)
D2	13.4	368	0.00193	411	0.00783	191
D3	21.5	590	0.00272	590	0.00625	190

TABLE 2: Default parameters of the CDP model under compound stress [10].

Parameter	Value
Dilatation angle	36°
Eccentricity	0.1
$f_{bo}/f_{co}$ (ratio of biaxial to uniaxial compressive strength)	1.16
K	0.667
Viscosity parameter	0

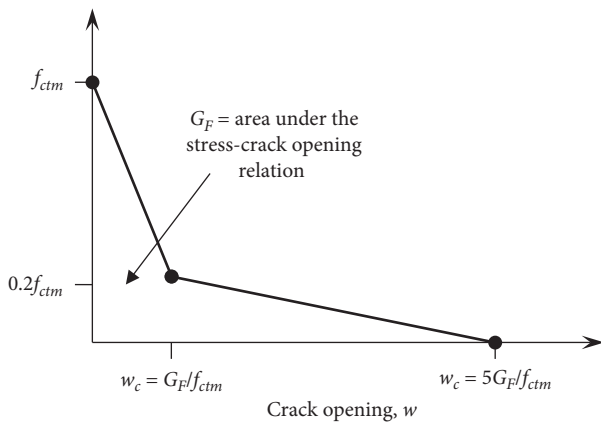


FIGURE 1: Stress-crack opening relation for uniaxial tension.

damage properties of concrete (Figure 2) were derived from a single known quantity average compressive strength of concrete ( $f_{cm}$ ).

**2.4. Finite Element Model Geometry, Mesh, and Boundary Condition.** The geometrical FEM of the flat RC slab supported on the column was plotted after the material properties were defined (Figure 3). The slab was supported on one edge by a shear wall and the opposite edge by columns. Overhanging slabs, equal to one-quarter of the panel dimension, were added on all noncontinuous sides to represent parts of the floor slabs of adjacent bays since the test specimen by [6] represents an interior panel of a prototype building. The center-to-center span length and thickness of the RC floor slabs were 1,630 mm in both directions and 56 mm, respectively, and the column dimensions were 136 mm × 136 mm with no capital.

In an FEM simulation, the mesh size is an essential factor in determining the validity of the analysis results. A coarse mesh can produce less precise outcomes while the finer mesh might extend the computation cost. There is no specific regulation on the mesh size. Therefore, an iterative method was employed to find the appropriate mesh size for the model. In the present study, a mesh size of 50 mm × 50 mm was appropriate to concrete and reinforcement bars generated using a mesh module (Figure 4).

The individual elements were connected properly after assembling all elements. The reinforcements were represented in the concrete region as embedded elements to ensure that the interactions between the reinforcement and concrete elements are fully bonded. The columns were directly tied to the slab using the option constraints embedment and tie.

The boundary conditions were developed using the boundary option with the initial step after the modeling and assembly of the section. The bottom surfaces of the supporting columns were fixed against all translation and rotation, and the slab nodes attached to the wall were restrained against translation in all directions (Figure 5).

**2.5. Model Loading Conditions.** The service gravity load was applied as a pressure force (Figure 6(a)) that was kept constant throughout the analysis, and the cyclic lateral load (Figure 6(b)) was applied with gradually increasing displacement amplitude using the loading spectrum (Figure 7) that provides more effective data regarding the hysteretic behavior of members or structures.

The vertical load applied to the RC floor slabs constituted a full-service live load of 3.8 kN/m<sup>2</sup> and an additional service dead load of 3.9 N/m<sup>2</sup>. A series of concentrated forces were applied, which were spaced at the center of 540 mm in each direction. A single vertical (gravity) load simulator controlled all point loads within one-panel width, including those in the quarter panel extension portions.

**2.6. FEM Validation.** The response of flat RC floor slabs without openings and slabs with different opening sizes, shapes, and locations was studied using FEM. Considering the accuracy and reliability of the numerical simulation software, the ultimate load and lateral displacement results of the flat RC floor slab in this study were extracted to verify the reliability of the model. The FEM results were compared to the experimental results obtained by [6]. The ultimate load and lateral displacement results are shown in Table 3, and the hysteretic curve for FEM and experiment results is shown in Figure 8. When the slab hysteretic curve, ultimate load, and lateral displacement obtained by FEM and experiment are compared, it is noticeable that the value estimated by the model deviates slightly from the experiment, but it is within the permissible range. Furthermore, the simulated hysteretic curve of the slab is essentially consistent with the experiment. As a result, the FEM result appears to be in excellent agreement with the experimental result.

**2.7. Parametric Study of Flat RC Slabs.** The parametric study examined the effects of different opening sizes, opening shapes, and opening locations of flat RC floor slabs subjected to cyclic in-plane and out-of-plane loads (Table 4).



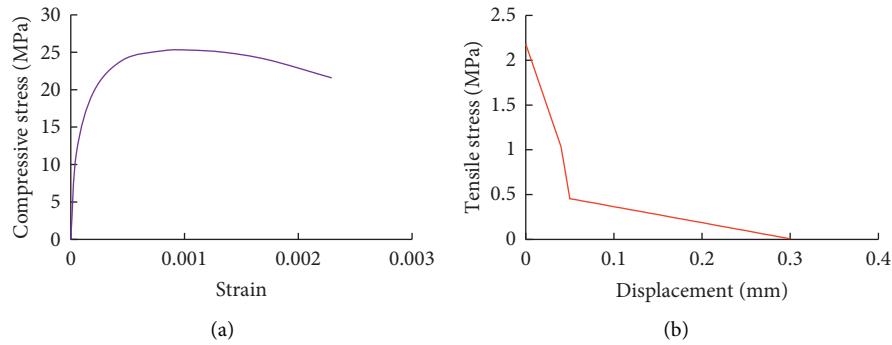


FIGURE 2: CDP model: (a) compressive behavior and (b) tensile behavior of the analyzed concrete.

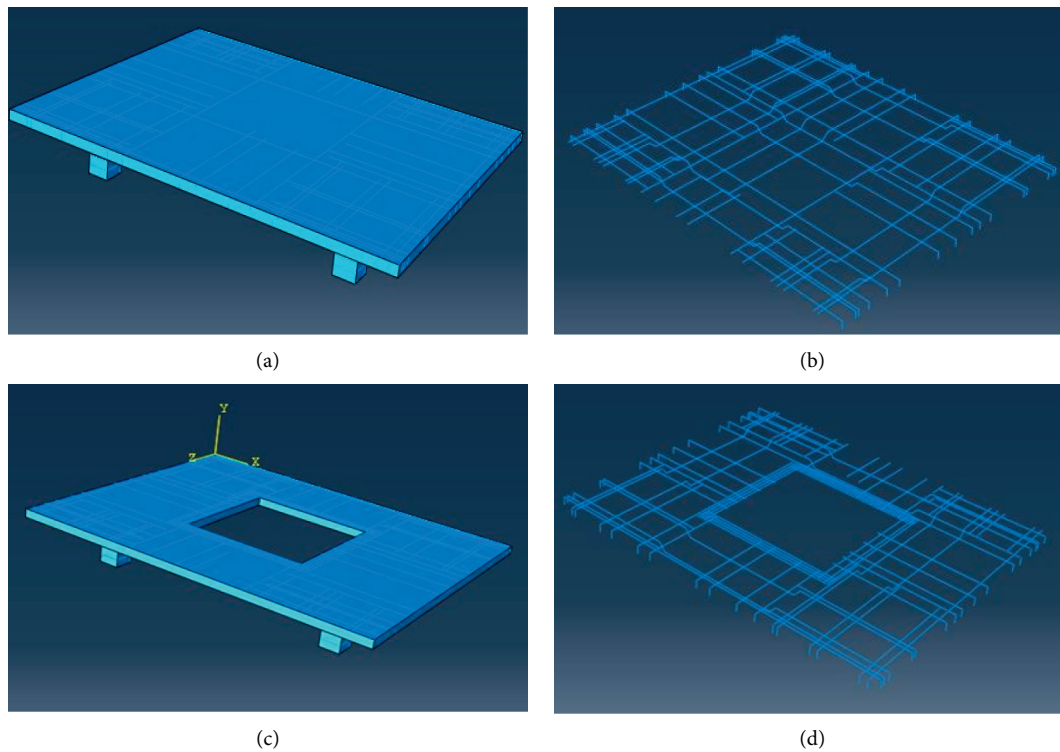


FIGURE 3: (a) Geometric model of a flat slab without opening, (b) embedded reinforcement of the flat slab without opening, (c) geometric model of a flat slab with opening, and (d) embedded reinforcement of the flat slab with opening.

To investigate the effect of opening size on flat RC slabs four different opening sizes were considered: 7%, 14%, 25%, and 30% of the total area of the slab. These openings were placed in the middle slab area. According to [12], any size of the opening is permitted in an area that is common to the intersecting middle strips if the requirements of both strength and serviceability are satisfied. In this study, half of the interrupted reinforcements were replaced on each side of the opening to maintain the full out-of-plane capacity of the slab.

The effect of the shape of the opening was investigated by considering elliptical, circular, L-shaped, T-shaped, cross, and rectangular openings (Figure 9). These openings were 14% of the total area of the slab found at the intersection of the two middle strips of the slab.

In the present study, three opening locations were selected. These were the intersection of two middle strips, the intersection of two-column strips, and the intersection of the middle and column strip.

### 3. Results and Discussion

**3.1. Effect of Opening Size on the Middle Strip of Flat RC Floor Slabs.** It can be seen from Figure 10 that as opening size increases in flat RC floor slab, there is a substantial decrease in its lateral load-carrying capacity. The numerical simulation shows that the inclusion of 30% opening in the floor slab causes a 68.54% drop in lateral load-carrying capacity of the floor slab system.

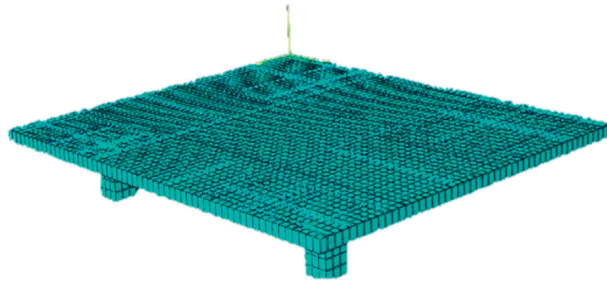


FIGURE 4: FEM mesh.

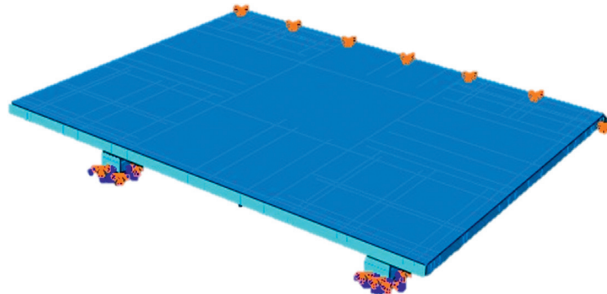


FIGURE 5: FEM boundary support conditions.

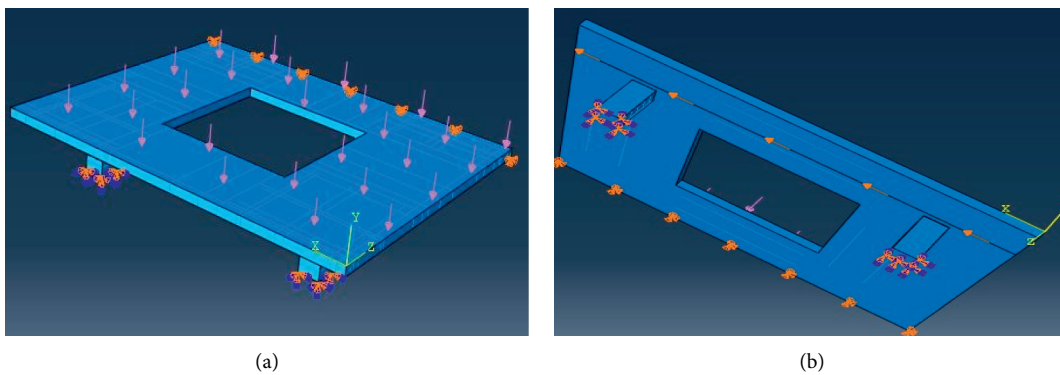


FIGURE 6: Loading conditions: (a) applied service load as a pressure and (b) applied displacement-based cyclic lateral load.

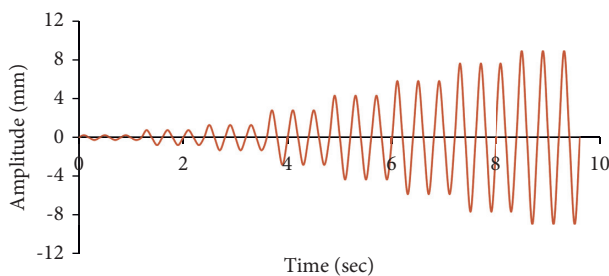


FIGURE 7: Cyclic loading history.

The relation between opening size and lateral load-carrying capacity can be expressed by the following equation using nonlinear regression:

$$y = 0.095x^2 - 5.638x + 124.87, \quad (2)$$

where  $y$  is the lateral load-carrying capacity (kN) and  $x$  is the opening size (%).

Figure 11 shows that lateral displacement decreases as opening sizes increase in flat floor slabs; it can be said that solid slabs (slab without opening) show high inelastic deformation compared to the one with an opening. From the present study, it can be observed that the inclusion of 30% opening causes a drop of 45.55% in stiffness.

The relation between opening size and lateral displacement can be expressed by equation (3) using nonlinear regression:

$$y = 0.0027x^2 - 0.164x + 5.6, \quad (3)$$

where  $y$  is the lateral displacement (mm) and  $x$  is the opening size (%).

The energy absorption capacity and stiffness of the floor slab decrease as the opening size gets higher (Figure 12).

TABLE 3: Comparison of FEM and experimental results.

Type of test	Parameters	FEM	Experiment
F1VCY [6]	Ultimate load (kN)	101.95	125.67
	Lateral displacement (mm)	4.19	5.61

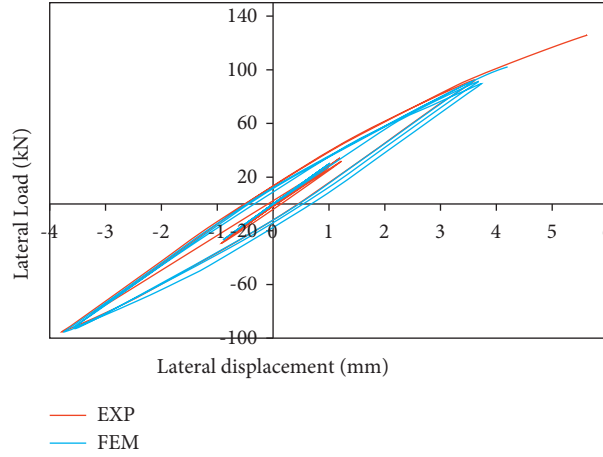


FIGURE 8: Comparison of hysteretic curves of experimental and FEM results.

TABLE 4: A summary of configurations adopted in the parametric study.

Opening sizes (%)	Opening shapes	Opening locations
0 (without opening)	Elliptical	The intersection of two middle strips
7	Circular	
14	L-shaped	The intersection of two-column strips
25	T-shaped	
30	Cross	The intersection of the middle and column strip
	Rectangular	

From this parametric study, the inclusion of 30% opening on the floor slab causes the drop of stiffness by 47.26%.

The relation between opening size and stiffness can be expressed by equation (4) using nonlinear regression:

$$y = -0.007x^2 - 0.115x + 22.541, \quad (4)$$

where  $y$  denotes stiffness (kN/mm) and  $x$  denotes the opening size (%).

**3.2. Effect of Opening Shape on the Middle Strip of Flat RC Floor Slabs.** Table 5 shows the effect of opening shapes on the middle strip lateral load-carrying capacity, lateral displacement, and stiffness of flat RC slabs. From the six types of opening shapes, a higher value of lateral load capacity and stiffness is seen in the circular opening shape. However, the cross-opening shape exhibits minimum lateral displacement.

**3.3. Effect of Opening Location on Flat RC Floor Slabs.** Varying the location of the opening higher value of lateral load-carrying capacity and inelastic deformation is observed

when the opening is provided at the intersection of two-column strips of the flat RC floor slab. Reduced lateral displacement is noticed where the opening is located at the intersection of two middle strips. Table 6 illustrates the effect of different opening locations.

**3.4. Sensitivity Analysis.** The combinations from the Latin hypercube sampling technique were modeled in Abaqus/CAE, and their lateral load capacity was determined (Table 7).

After the determination of the lateral load-carrying capacity, regression is done to relate the input parameters or find the correlation coefficient as follows:

$$y = -0.383P_d - 2.897O_p + 0.458C + 0.013S + 95.767, \quad (5)$$

where  $y$  denotes the lateral load capacity,  $P_d$  is the service load,  $O_p$  is the opening size,  $C$  is the compressive strength of concrete, and  $S$  is the steel reinforcement strength.

From the regression analysis, it is revealed that opening size is the most influential factor in decreasing the lateral

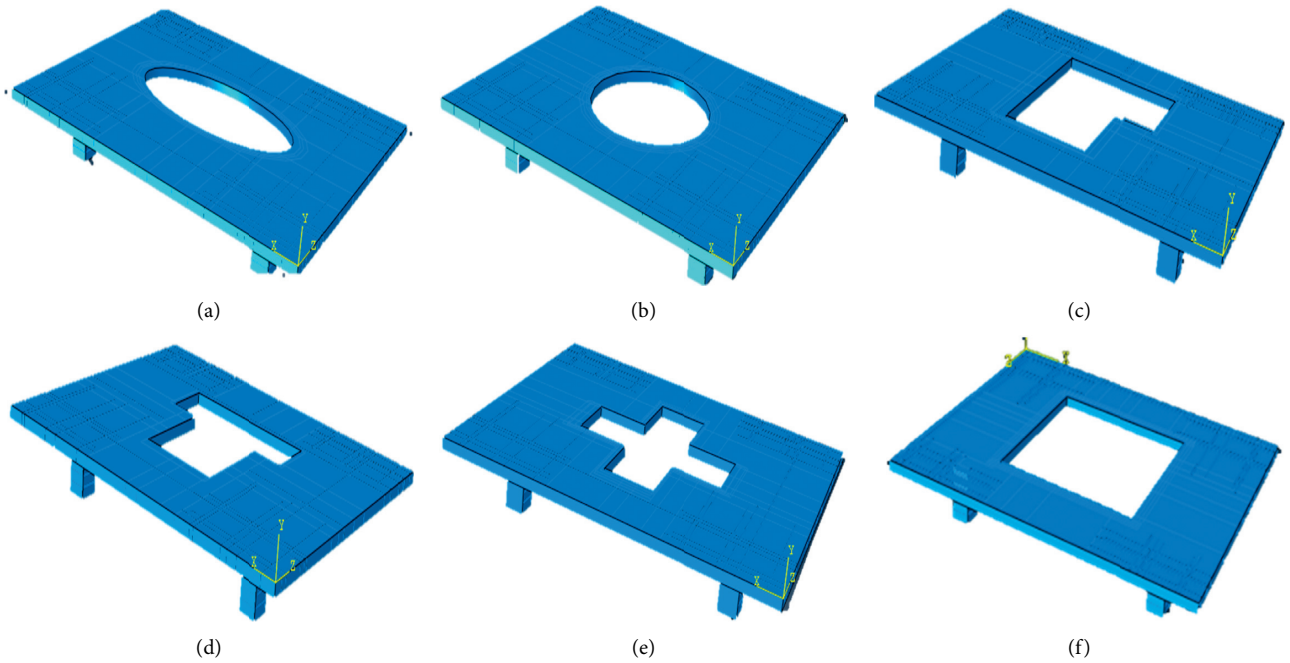


FIGURE 9: Flat RC floor slab with different opening shapes: (a) elliptical opening, (b) circular opening, (c) L-shaped opening, (d) T-shaped opening, (e) cross opening, and (f) rectangular opening.

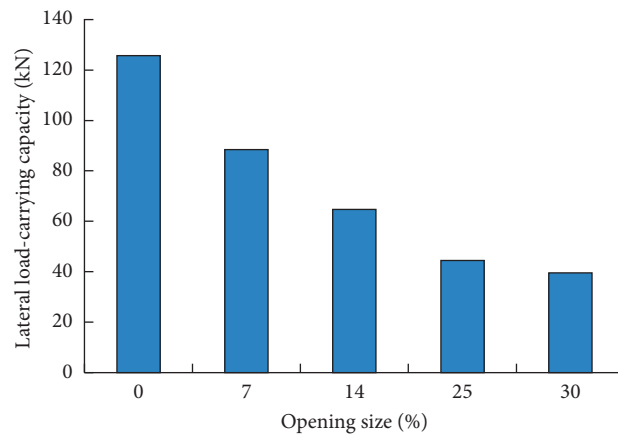


FIGURE 10: Effect of opening size on the lateral load capacity of the RC floor slab.

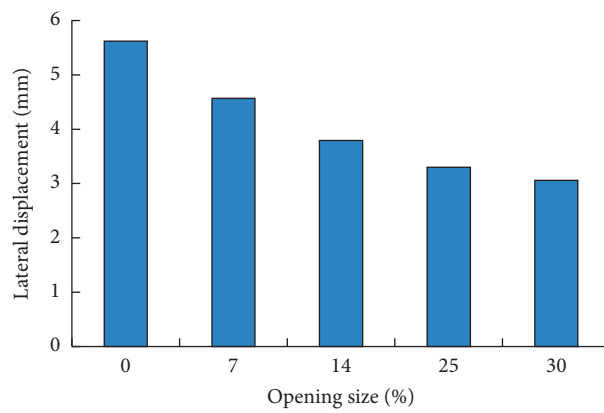


FIGURE 11: Effect of opening size on the lateral displacement of the floor slab.

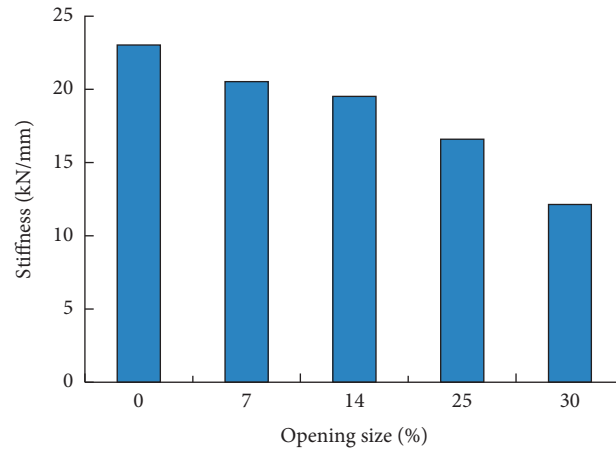


FIGURE 12: Effect of opening size on the stiffness of the floor slab.

TABLE 5: Effect of different opening shapes.

Opening shape	Lateral load-carrying capacity (kN)	Lateral displacement (mm)	Stiffness (kN/mm)
Rectangular	64.82	3.30	19.53
Elliptical	72.62	3.37	21.50
Circular	73.77	3.53	22.49
L-shaped	55.77	3.43	17.06
Cross	68.12	2.71	20.93
T-shaped	55.60	3.25	20.75

TABLE 6: Effect of different opening locations.

Opening location	Lateral load-carrying capacity (kN)	Lateral displacement (mm)	Stiffness (kN/mm)
The intersection of two middle strips	64.82	3.30	19.53
The intersection of two-column strips	75.09	3.64	21.40
Intersection of the middle and column strip	70.33	3.37	20.54

TABLE 7: The lateral load-carrying capacity of RC floor slabs from the Latin hypercube result.

Compos	Lateral load capacity (kN)	Compos	Lateral load capacity (kN)
1	53.72	17	50.97
2	43.95	18	52.17
3	41.62	19	65.94
4	57.15	20	54.61
5	56.48	21	49.6
6	52.68	22	68.21
7	59.52	23	62
8	56.38	24	52.89
9	54.97	25	79.47
10	43.37	26	64.97
11	40.6	27	47.72
12	50.31	28	63.13
13	43.28	29	71.01
14	49.19	30	51.08
15	47.67	31	50.46
16	62.73	32	75.18

load capacity of the RC floor slab since it has a higher correlation coefficient.

#### 4. Conclusion

The nonlinear FEA was used to investigate the response of flat RC floor slabs subjected to cyclic in-plane loading. The influence of the slabs' aspect ratio, opening size, location, and shape was evaluated. To analyze the hysteretic behavior of concrete slabs, numerical simulation using FEA software, Abaqus/CAE, is capable of producing accurate and suitable estimations. Six types of opening shapes located on the middle panel of the floor slab were included. The energy absorption capacity and stiffness of RC floor slabs can be affected by the presence of openings. However, from these opening shapes, better energy absorption capacity and stiffness were observed in circular ones. The opening located at the intersection of two-column strips near the shear wall support showed better performance compared with the two other locations. It can be concluded that small opening sizes are recommended especially in earthquake-prone areas since the seismic capacity of the floor diaphragm is greatly affected by the presence of openings.

#### Data Availability

The data used to support the findings of this study are available from the corresponding author upon request.

#### Conflicts of Interest

The authors declare that they have no conflicts of interest.

#### References

- [1] R. Khajehdehi and N. Panahshahi, "Effect of openings on in-plane structural behavior of reinforced concrete floor slabs," *Journal of Building Engineering*, vol. 7, pp. 1–11, 2016.
- [2] F. C. Wolfgram and B. Alireza, "Contribution of RC floor slabs in resisting lateral loads," *Journal of Structural Engineering*, vol. 115, no. 1, pp. 1–18, 1989.
- [3] A. U. Rahman, A. Prof, and N. Jamshetty, "Seismic effect of rigid floor diaphragm," *International Research Journal of Engineering and Technology*, vol. 6, pp. 433–441, 2019.
- [4] B. M. Moeini and B. Rafezy, "Investigation into the floor diaphragms flexibility in reinforced concrete structures and code provision," *Global Journal of Researches in Engineering*, vol. 11, no. 1, 2011.
- [5] E. Thomas, J. George, D. Paulose, M. Tech, C. Engineering, and A. Jyothi, "Assessment of the diaphragm condition for the floor systems," *International Research Journal of Engineering and Technology*, vol. 4, no. 6, pp. 836–843, 2017.
- [6] S. Chen, *Reinforced Concrete Floor Slabs under In-Plane Monotonic and Cyclic Loading*, Lehigh University, Bethlehem, PA, USA, 1986.
- [7] R. Khajehdehi and N. Panahshahi, "Nonlinear FE analysis of RC building floor diaphragms with openings subjected to in-plane and out-of-plane loads," in *NCEE 2014 - 10th US National Conference on Earthquake Engineering Front Earthquake Engineering*, p. 66045, Anchorage, Alaska, USA, July 2014.
- [8] B. S. Taranath, *Wind and Earthquake Resistant Buildings: Structural Analysis and Design*, CRC Press, Boca Raton, FL, USA, 2004.
- [9] Y. Sümer and M. Aktaş, "Defining parameters for concrete damage plasticity model," *Challenge Journal of Structural Mechanics*, vol. 1, no. 3, pp. 149–155, 2015.
- [10] P. Kmieciak and M. Kamiński, "Modelling of reinforced concrete structures and composite structures with concrete strength degradation taken into consideration," *Archives of Civil and Mechanical Engineering*, vol. 11, no. 3, pp. 623–636, 2011.
- [11] Abaqus/Cae, *Abaqus/Cae User's Manual*, Dassault Systèmes Simulia Corp., Providence, RI, USA, 2011.
- [12] AcI 318 Ac, *Building Code Requirements for Structural Concrete (ACI 318-05) and Commentary (ACI 318r-05)*, American Concrete Institute, Farmington Hills, MI, USA, 2005.